Research Square

Preprints are preliminary reports that have not undergone peer review.
They should not be considered conclusive, used to inform clinical practice,
or referenced by the media as validated information.

Emergent asperity localization enables physics-based prediction of surface rupture displacement

Jia Cheng

jiacheng@cugb.edu.cn

China University of Geosciences, Beijing

Xi-Wei Xu

Institute of Geology China Earthquake Administration https://orcid.org/0000-0002-8301-7347

Article

Keywords:

Posted Date: August 11th, 2026

DOI: https://doi.org/10.21203/rs.3.rs-9453717/v1

License: This work is licensed under a Creative Commons Attribution 4.0 International License.
Read Full License

Additional Declarations: There is **NO** Competing Interest.

Emergent asperity localization enables physics-based prediction of surface rupture displacement

Jia Cheng*, Xiwei Xu*

Abstract

Surface rupture displacement is a critical parameter controlling earthquake-related damage and fault-specific seismic hazard, yet its along-strike variability remains difficult to predict. Existing approaches commonly rely on empirical scaling relationships or prescribe heterogeneous stress and frictional conditions, leaving unresolved whether localized high-slip domains, or asperities, are fundamental consequences of earthquake physics or simply imposed model assumptions.

Here we develop a physics-based framework in which asperity-like slip localization emerges naturally from the constraints imposed by seismic moment conservation and finite fault geometry. By coupling a moment-balanced truncated Gutenberg–Richter earthquake occurrence model with magnitude-dependent rupture scaling, we show that uniform slip distributions become unstable under a fixed moment budget, and localized slip domains arise as energetically preferred configurations without prescribing asperity locations or heterogeneous frictional patches.

The framework reproduces the observed spatial organization of surface rupture displacement across 23 historical strike-slip earthquakes, capturing both segmented and throughgoing rupture patterns across diverse tectonic environments. Applications to the central San Andreas Fault and the Anninghe Fault further demonstrate that fault-specific displacement distributions can be predicted from fault geometry, slip rate, and seismic moment constraints alone.

Our results reveal that asperity localization is not merely an inherited feature of fault heterogeneity, but an emergent property of finite fault systems. This provides a unified physical basis for predicting surface rupture displacement and improves the mechanistic understanding of earthquake rupture complexity and fault-specific seismic hazard.

State Key Laboratory of Deep Earth Exploration and Imaging, School of Earth Sciences and Resources, China University of Geosciences (Beijing), Beijing 10083, China

* Corresponding author: Jia Cheng, jiacheng@cugb.edu.cn); Xiwei Xu, xiweixu@vip.sina.com

Introduction

Surface rupture displacement represents one of the most direct expressions of earthquake faulting and is a critical parameter for assessing earthquake-induced damage to infrastructures, lifelines, and fault-crossing facilities[1-4]. Unlike earthquake magnitude or seismic moment, which provide integrated measures of rupture size, surface displacement exhibits strong along-strike variability controlled by rupture segmentation, fault geometry, and the spatial distribution of coseismic slip. Empirical studies based on geological observations have established relationships between earthquake magnitude, rupture dimensions, and maximum surface displacement[1,5]. However, large variability remains among earthquakes with comparable magnitudes, indicating that displacement patterns cannot be fully explained by magnitude-dependent scaling alone[1,6]. Understanding the physical origin of this variability is therefore essential for improving fault-specific seismic hazard assessment[1].

Spatially heterogeneous slip distributions are widely observed in large earthquakes, with localized high-slip regions commonly referred to as asperities or slip concentrations[7-10]. These localized domains strongly influence rupture propagation, near-field ground motion, and surface displacement patterns[11,12]. Consequently, asperity structure has become a fundamental component in earthquake source characterization and strong-motion simulation.

However, in most existing earthquake rupture models, asperities are introduced as prescribed heterogeneities in initial stress, frictional properties, or slip distributions rather than being derived from fundamental physical constraints[5,8,11-17]. Although such approaches successfully reproduce complex rupture observations, they leave an important question unresolved: are asperity-controlled slip patterns merely inherited from imposed fault heterogeneity[16-19], or can localized slip emerge naturally from the physical constraints governing earthquake rupture?

Dynamic rupture simulations have provided important insights into the relationship between stress heterogeneity, frictional behavior, and rupture complexity [10-12]. These models demonstrate that heterogeneous rupture patterns can arise from nonlinear interactions between rupture dynamics and fault properties. However, realistic simulations generally require detailed knowledge of spatially variable stresses,

friction parameters, and constitutive laws that are rarely available for natural faults. As a result, predicting the spatial distribution of surface rupture displacement on individual active faults remains challenging[1,2,5,20].

From a broader perspective, earthquake rupture is constrained by fundamental conservation principles. The seismic moment released during earthquakes must balance the long-term tectonic loading accumulated on finite fault systems[21,22]. This constraint links earthquake occurrence statistics, rupture dimensions, and cumulative fault deformation. Yet whether such global constraints alone can generate localized slip structures analogous to asperities has not been systematically explored.

Here we develop a physics-based framework to investigate whether asperity-like slip localization can emerge as a consequence of seismic moment conservation and finite fault geometry. Instead of prescribing asperity locations, heterogeneous frictional patches, or target slip distributions, we formulate earthquake occurrence using a moment-balanced truncated Gutenberg–Richter relationship[21] and combine it with magnitude-dependent rupture scaling[20,23]. Within this framework, the slip distribution evolves toward localized configurations that satisfy the seismic moment constraint while minimizing the system energy.

We show that localized slip domains emerge naturally from the constrained rupture system and provide a physical explanation for the formation of asperity-controlled displacement patterns. The resulting framework links long-term tectonic loading, earthquake statistics, rupture geometry, and surface displacement within a unified formulation (Figure 1).

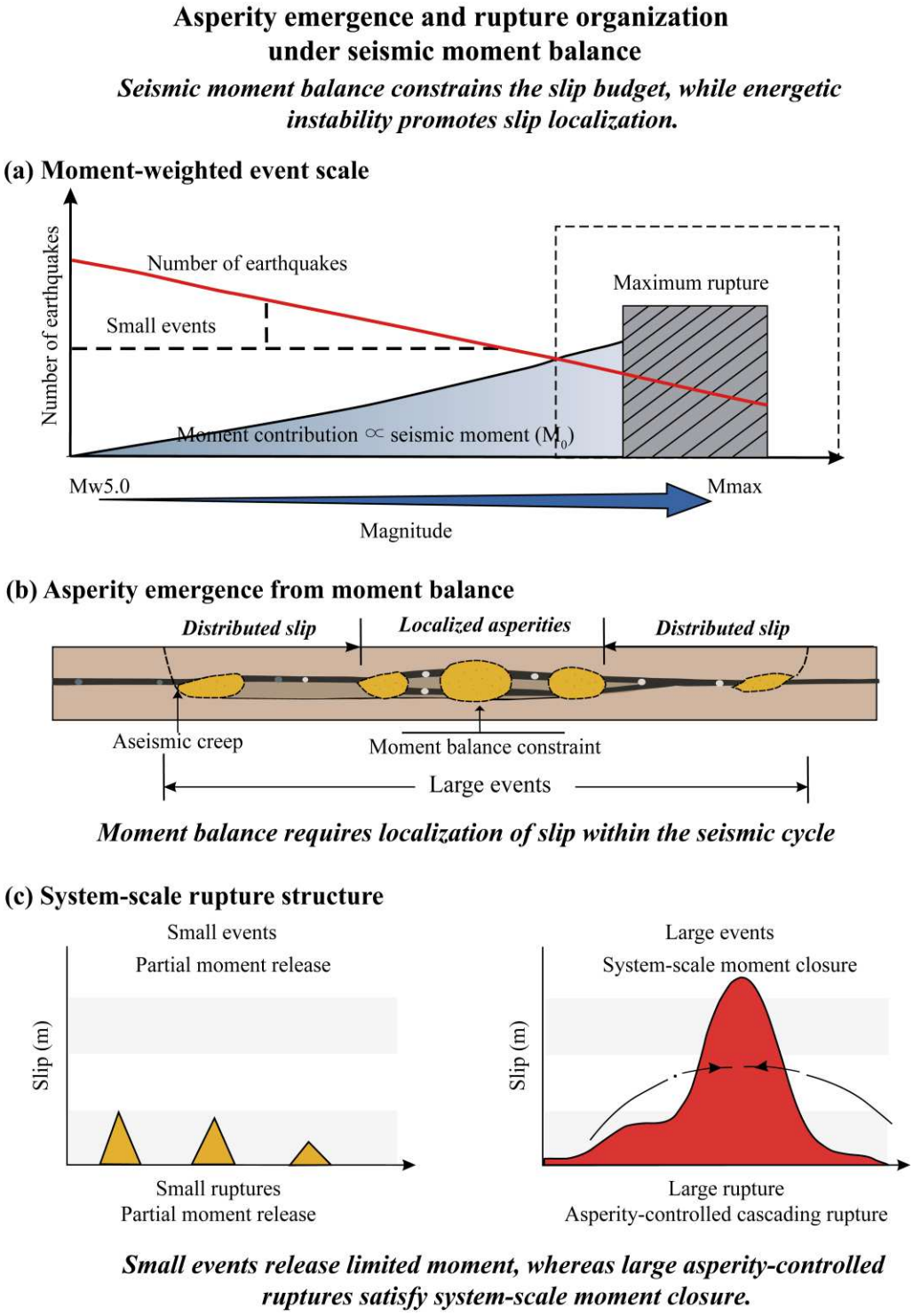


Figure 1 | Emergence of asperities and rupture organization under seismic moment balance. a, Moment-weighted earthquake scaling on a finite fault. The number of earthquakes decreases with increasing magnitude following a truncated Gutenberg–Richter distribution, whereas the contribution to seismic moment increases strongly toward large events. The maximum magnitude, Mmax, is constrained by the finite fault geometry and the corresponding maximum rupture dimensions. The

intersection between earthquake frequency and moment contribution illustrates the increasing dominance of large events in the seismic-cycle moment budget. **b,** Emergent localization of slip under the moment-balance constraint. Although tectonic loading is distributed along the fault, the requirement to accommodate the seismic-cycle moment budget allows slip to become spatially concentrated into localized high-slip domains (asperities). Aseismic creep and distributed deformation can accommodate part of the long-term loading, while the remaining seismically released moment is preferentially concentrated within asperity domains. **c,** System-scale organization of rupture. Small earthquakes release only a fraction of the available seismic moment and produce spatially distributed, partial rupture. In contrast, large earthquakes can link neighboring localized slip domains and produce asperity-controlled cascading rupture, resulting in system-scale moment release and coherent, localized slip. Together, these conceptual relationships motivate the central hypothesis of this study: asperity localization and the organization of large earthquake rupture can emerge from the interaction between finite-fault geometry and seismic moment balance, rather than requiring asperity locations to be prescribed a priori.

Results

We validate the framework against 23 historical strike-slip earthquakes, including both isolated intraplate ruptures and multi-segment plate-boundary earthquakes, demonstrating that emergent asperity localization reproduces the observed along-strike variability of surface rupture displacement. We further apply the model to the central San Andreas Fault[24,25] and the Anninghe Fault[26,27] to evaluate its predictive capability for active fault systems. Our results suggest that asperity localization is not necessarily an externally imposed property of fault heterogeneity, but can arise as an emergent characteristic of finite fault systems governed by seismic moment constraints.

This finding provides a new physical perspective for understanding rupture complexity and establishes a mechanism-based approach for predicting fault-specific surface rupture displacement.

Slip localization emerges naturally from constrained energy minimization

A fundamental question in earthquake rupture physics is whether asperity-like slip concentrations represent externally imposed fault heterogeneity or whether they can emerge from the intrinsic constraints governing finite fault systems. To address this question, we first examine the stability of slip distributions under a fixed seismic

moment constraint. Rather than prescribing spatially variable frictional properties or predefined high-slip regions, we formulate a reduced-order variational framework in which the slip field evolves toward energetically preferred configurations while conserving the total seismic moment[7,10].

For a finite fault discretized into N sub-faults, the seismic moment constraint requires that

$$M_0 = \sum_i \mu A_i D_i \tag{2}$$

where D_i, A_i, and μ represent slip, sub-fault area, and rigidity, respectively. A spatially uniform slip distribution satisfies this constraint, but it does not necessarily represent the most stable configuration of the system. Small perturbations that redistribute slip while conserving the total moment can reduce the system energy by concentrating deformation into localized regions. This instability provides a physical pathway through which asperity-like structures may emerge without prescribing their locations (Figure 2a).

To explore this behavior, we define a constrained energy functional:

$$\prod[D] = E_{elastic}[D] + E_{friction}[D] + \lambda(\textstyle\sum_i \mu A_i D_i - M_0) \tag{2}$$

where the Lagrange multiplier λ ensures conservation of seismic moment during the optimization process. The slip distribution evolves through iterative minimization of this constrained functional, with the slip field updated toward configurations that reduce the total energy while maintaining the prescribed moment budget.

The resulting energy landscape reveals a transition from a homogeneous slip configuration toward localized states with lower system energy (Figure 2b). The uniform configuration corresponds to a reference high-energy state, whereas localized solutions represent energetically preferred configurations within the constrained system. Importantly, the schematic energy landscape is not intended to represent an empirical potential function or a prescribed double-well fracture model. Instead, it illustrates the local bifurcation behavior of the constrained system: a homogeneous solution becomes unstable, and perturbations grow toward localized slip states (Figure 2b).

We further demonstrate this localization process through numerical evolution of the constrained minimization (Figure 2c). Starting from an approximately uniform slip distribution with small perturbations, the slip field gradually develops spatial concentration without imposing asperity positions, peak slip values, or heterogeneous

frictional patches. The initially small perturbations are amplified during the optimization process, resulting in the spontaneous formation of localized high-slip domains. These localized structures emerge from the interaction between the moment constraint and the finite spatial extent of the fault system.

To quantify this transition, we introduce a slip localization index:

$$LI = \frac{\sqrt{\frac{1}{N}\sum_i (D_i - \overline{D})^2}}{\overline{D}} \tag{3}$$

where $\overline{D}$ represents the mean slip over the fault surface. A perfectly uniform slip distribution has LI =0, whereas increasing LI indicates progressively stronger slip localization. During the minimization process, the normalized system energy decreases while the localization index increases, indicating that the system evolves from a homogeneous configuration toward a stable localized solution (Figure 2d).

The emergence of localization is not dependent on a unique initial perturbation pattern. Repeated simulations with different small perturbations produce comparable localized solutions in terms of energy reduction and slip concentration, although the exact spatial positions of localized domains may vary. This behavior indicates that asperity-like structures arise as a consequence of the instability of the homogeneous solution rather than from externally prescribed fault heterogeneity.

The variational demonstration provides a physical basis for the subsequent rupture simulations. In the full earthquake occurrence framework, the emergent localization behavior is incorporated through finite fault geometry, rupture scaling relationships, and seismic moment conservation[20,21,27]. The resulting rupture scenarios therefore inherit the same physical principle: slip concentration is governed by the constraints of the fault system rather than imposed spatial patterns. This provides a mechanistic explanation for why localized displacement patterns are repeatedly observed in natural strike-slip earthquakes[1,1].

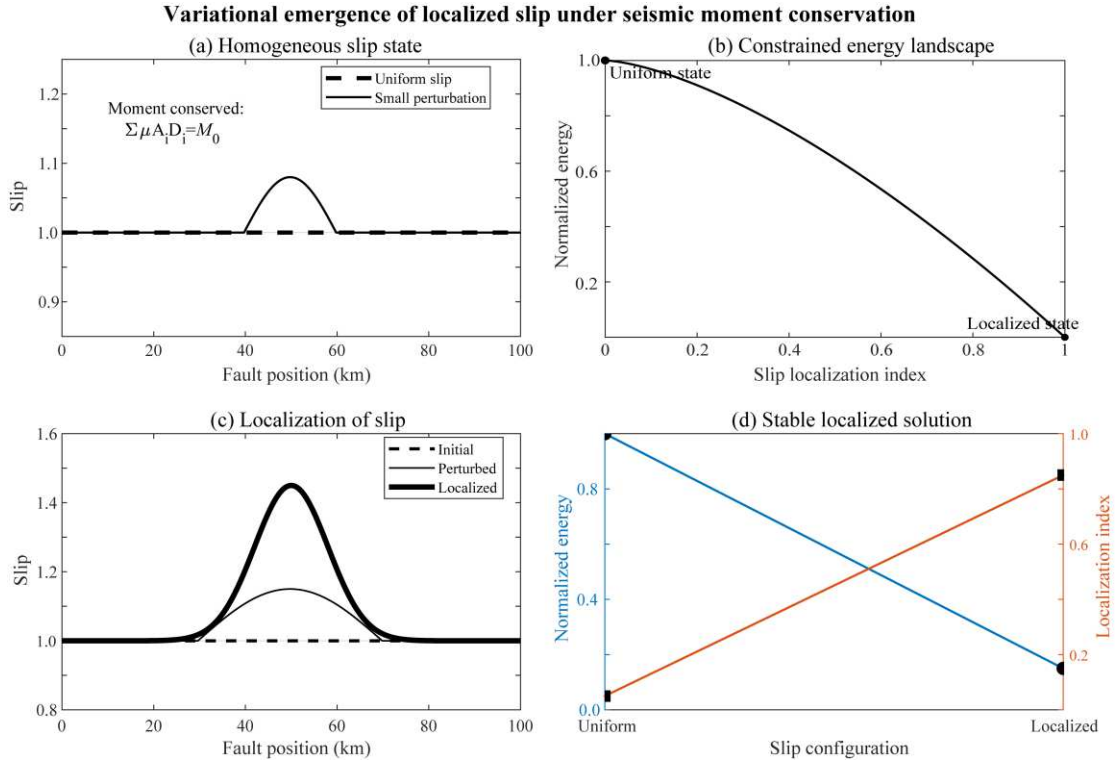


Figure 2 | Variational emergence of localized slip under seismic moment conservation. a, A homogeneous slip distribution satisfies the seismic moment constraint but represents a mechanically unstable configuration. Small perturbations can trigger redistribution of slip under the constrained energy landscape. b, Reduced-order variational formulation of slip localization. The effective energy functional combines nonlinear localization and spatial smoothing terms while enforcing seismic moment conservation. The energy landscape illustrates the transition from homogeneous slip toward energetically preferred localized states. c, Numerical evolution of the slip field during constrained minimization. Starting from a perturbed homogeneous distribution, slip progressively concentrates into localized high-slip domains without prescribing the final slip pattern. d, Evolution of the normalized system energy and localization index during minimization. Energy reduction accompanies increasing slip localization, demonstrating that localized slip configurations represent stable solutions under a fixed moment constraint.

Observation-based validation of emergent asperity-controlled rupture patterns

To evaluate whether the proposed framework captures the first-order characteristics of natural earthquake rupture, we applied the model to 23 historical strike-slip earthquakes spanning a wide range of magnitudes, rupture lengths, fault geometries, and tectonic environments (Supplementary Table S2). The earthquake dataset includes both isolated intracontinental ruptures and complex multi-segment plate-boundary earthquakes, providing an independent benchmark for assessing the generality of the model. Model parameters were determined from fault geometry, long-

term slip rate, and the moment-balanced earthquake occurrence model, without calibrating asperity locations or surface displacement distributions against individual earthquakes[1,21,28,29].

For each earthquake, rupture dimensions were estimated using the magnitude-dependent scaling relationship, and the cumulative rupture probability was derived from the truncated Gutenberg–Richter recurrence model constrained by the long-term tectonic moment rate. Localized rupture displacement was subsequently calculated by integrating rupture occurrence over the complete seismic cycle while conserving the cumulative seismic moment. Consequently, the predicted displacement patterns arise from the interaction among fault segmentation, rupture scaling, and seismic moment conservation, rather than from prescribed heterogeneous slip distributions[20,21,26].

Figure 3 compares the modeled rupture characteristics with geological and geodetic observations for four representative earthquakes: the 2001 Mw 7.8 Kunlun earthquake, the 2021 Mw 7.4 Maduo earthquake, the 2023 Mw 7.8 Türkiye earthquake, and the 2025 Mw 7.7 Mandalay earthquake. These events represent a broad spectrum of rupture behaviors, including isolated continental ruptures, segmented intracontinental earthquakes, and multi-segment plate-boundary ruptures[30-37]. For each earthquake, the first row illustrates the cumulative spatial distribution of earthquake occurrence derived from the moment-balanced recurrence model. Regions with elevated cumulative occurrence correspond to portions of the fault that experience repeated participation in rupture over successive seismic cycles. Because larger ruptures intersect these locations more frequently, cumulative rupture participation becomes spatially concentrated within specific portions of the fault system[28,29].

The second row presents the modeled cumulative rupture displacement. Despite the absence of prescribed asperity locations, the simulations consistently generate localized high-displacement domains rather than spatially uniform slip accumulation. These localized domains are primarily controlled by fault segmentation and rupture interaction. On relatively simple faults such as the Kunlun rupture, the model predicts one dominant localized slip domain occupying the central portion of the rupture. In contrast, geometrically complex systems, including the Türkiye and Mandalay earthquakes, develop multiple localized displacement domains associated with adjacent fault segments. These results indicate that rupture complexity emerges naturally from finite fault geometry rather than requiring distinct physical mechanisms for different tectonic settings[30-39].

The third row compares the predicted surface rupture displacement with field measurements and remote-sensing observations. The model successfully reproduces the first-order along-strike variability of observed displacement, including the locations of principal displacement maxima and the gradual reduction of slip toward rupture terminations. Although local discrepancies remain because secondary faulting, shallow sediment deformation, and site-specific geological effects are not explicitly represented, the predicted displacement envelopes closely follow the observed spatial organization for all four earthquakes[30,31-37,40].

Importantly, the same parameterization was applied throughout the complete earthquake dataset. No earthquake-specific adjustment was introduced to reproduce individual displacement profiles. Instead, the observed variability arises from differences in fault length, segmentation geometry, rupture dimensions, and cumulative seismic moment budget. This demonstrates that localized rupture displacement can be explained using a unified physical framework, rather than by prescribing event-dependent asperity distributions[1].

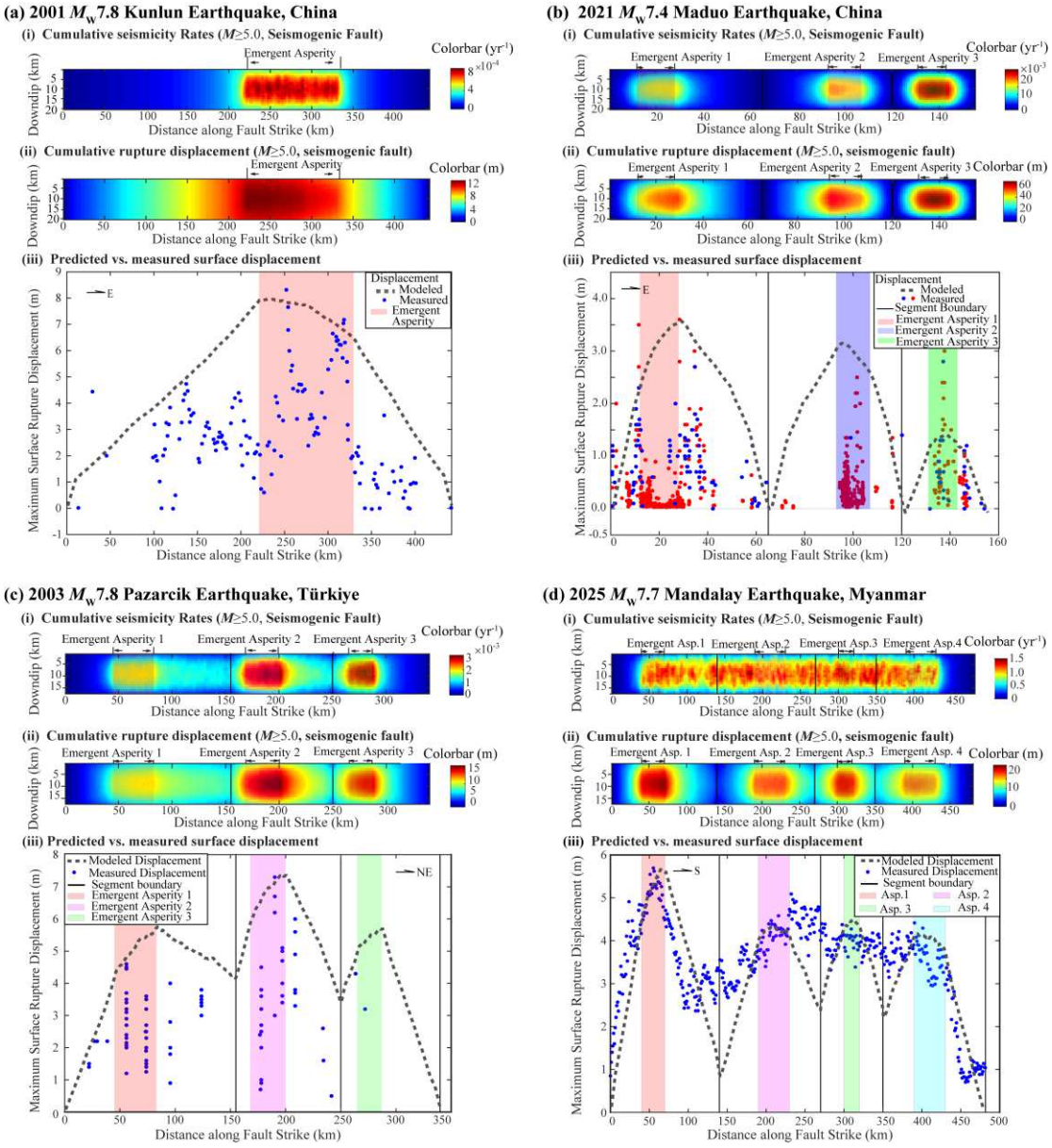


Figure 3 | Observation-based validation of asperity-controlled rupture patterns across strike-slip earthquakes. **a–d,** Comparison between simulated and observed rupture characteristics for four large strike-slip earthquakes spanning different tectonic settings: **(a)** the 2001 Mw7.8 Kunlun earthquake, China; **(b)** the 2021 Mw7.4 Maduo earthquake, China; **(c)** the 2003 Mw7.8 Pazarcık earthquake, Türkiye; and **(d)** the 2025 Mw7.7 Mandalay earthquake, Myanmar. **(i)** Spatial distribution of cumulative seismicity rates derived from the moment-balanced earthquake occurrence model. Localized zones of enhanced seismic productivity correspond to regions where rupture interaction and slip accumulation are concentrated. **(ii)** Predicted cumulative rupture displacement distribution along the finite fault system. Localized high-slip domains emerge from the combination of rupture scaling, seismic moment conservation, and fault segmentation. **(iii)** Comparison between modeled and observed surface rupture displacement. The predicted displacement profiles reproduce the first-order spatial variability and peak displacement locations observed in geological measurements and remote-sensing investigations. Colored regions indicate asperity domains inferred from

the modeled localization patterns. Together, these results demonstrate that asperity-controlled rupture patterns provide a unified explanation for along-strike displacement variability across both isolated intraplate earthquakes and multi-segment plate-boundary ruptures.

To quantify model performance, we compared the predicted and observed maximum surface displacements for all 23 historical earthquakes (Extended Data Fig. 1Extended Data Fig. 19, and Supplementary Table S3). The predicted values show strong agreement with geological observations over nearly two orders of magnitude in displacement, indicating that the model captures the dominant controls on fault-scale rupture variability. The remaining residuals exhibit no systematic dependence on earthquake magnitude or tectonic environment, suggesting that the proposed framework is broadly applicable across diverse strike-slip fault systems[30-40].

Collectively, these results demonstrate that emergent asperity localization provides a consistent physical explanation for the observed spatial variability of surface rupture displacement. Rather than representing predefined structural features, localized high-slip domains arise as natural consequences of finite fault geometry, cumulative tectonic loading, and seismic moment conservation, thereby linking long-term earthquake occurrence with coseismic surface deformation within a single predictive framework[7,9,10].

Physics-based prediction of surface rupture displacement on active faults

Having demonstrated that the proposed framework reproduces the principal characteristics of historical strike-slip earthquakes without event-specific calibration, we next evaluate its predictive capability for active fault systems whose future rupture behavior remains uncertain. Unlike retrospective validation, this application represents a forward prediction in which only geological fault geometry, long-term slip rate, and earthquake occurrence statistics are specified prior to simulation.

Two representative segmented strike-slip faults were selected: the central San Andreas Fault in California and the Anninghe Fault in southwestern China (Figure 4). These two fault systems exhibit contrasting tectonic environments and segmentation characteristics. The San Andreas Fault forms a mature plate-boundary fault with long, laterally continuous fault strands, whereas the Anninghe Fault is an intracontinental strike-slip fault characterized by relatively short structural segments and pronounced geometric discontinuities. Together, these systems provide an opportunity to evaluate

whether a unified physical framework can predict rupture displacement across different styles of fault segmentation.

For each fault, geological segmentation defines the finite rupture geometry used in the simulations (Figure 4a, b, panel i). Earthquake recurrence is determined using the moment-balanced truncated Gutenberg–Richter relationship constrained by the mapped fault length, down-dip width, and long-term slip rate. Magnitude-dependent rupture dimensions are subsequently calculated using empirical rupture-scaling relations, allowing earthquake ruptures of different sizes to interact with the segmented fault geometry throughout successive seismic cycles.

The cumulative rupture displacement distributions predicted by the model are shown in Figure 4a,b (panel ii). Rather than producing spatially uniform deformation, the simulations consistently generate localized high-displacement domains whose locations are governed by rupture overlap within the segmented fault system. Importantly, these localized regions are not imposed as predefined asperities. Instead, they emerge naturally from the combined effects of finite fault geometry, rupture scaling, and cumulative seismic moment conservation. Fault sections that repeatedly participate in ruptures over the seismic cycle progressively accumulate greater displacement, whereas geometrically isolated sections experience comparatively lower cumulative deformation.

The resulting surface rupture displacement profiles are presented in Figure 4a,b (panel iii). Both fault systems exhibit pronounced along-strike variability despite having relatively uniform long-term slip rates. Peak displacement is concentrated within several localized domains, while displacement decreases toward segment boundaries and rupture terminations. The predicted patterns therefore indicate that fault segmentation strongly modulates the spatial distribution of surface rupture even under identical regional tectonic loading.

The predicted behavior differs systematically between the two fault systems. On the central San Andreas Fault, the relatively continuous fault geometry promotes broader interaction among neighboring ruptures, producing wider localized displacement domains with comparatively smooth spatial transitions. In contrast, the Anninghe Fault exhibits stronger localization associated with individual fault segments, reflecting reduced rupture connectivity across geometric discontinuities. These contrasting patterns arise naturally from differences in fault geometry rather than from

tectonic setting itself, suggesting that rupture localization is fundamentally controlled by the spatial organization of finite fault systems.

Although no future earthquake observations currently exist for direct comparison, the predicted displacement distributions are physically consistent with the rupture characteristics observed in historical strike-slip earthquakes presented in Figure 3. In both retrospective and prospective applications, localized surface displacement develops through the same physical mechanism, namely the interaction between earthquake recurrence, rupture scaling, and seismic moment conservation. The predictive simulations therefore extend the validated physical framework from historical earthquake reconstruction to fault-specific hazard assessment.

These results demonstrate that localized rupture displacement can be estimated directly from measurable geological quantities without prescribing asperity locations or event-specific slip distributions. Consequently, the proposed framework provides a practical tool for evaluating the spatial variability of future surface rupture on active strike-slip faults and establishes a physically interpretable basis for displacement-based seismic hazard assessment.

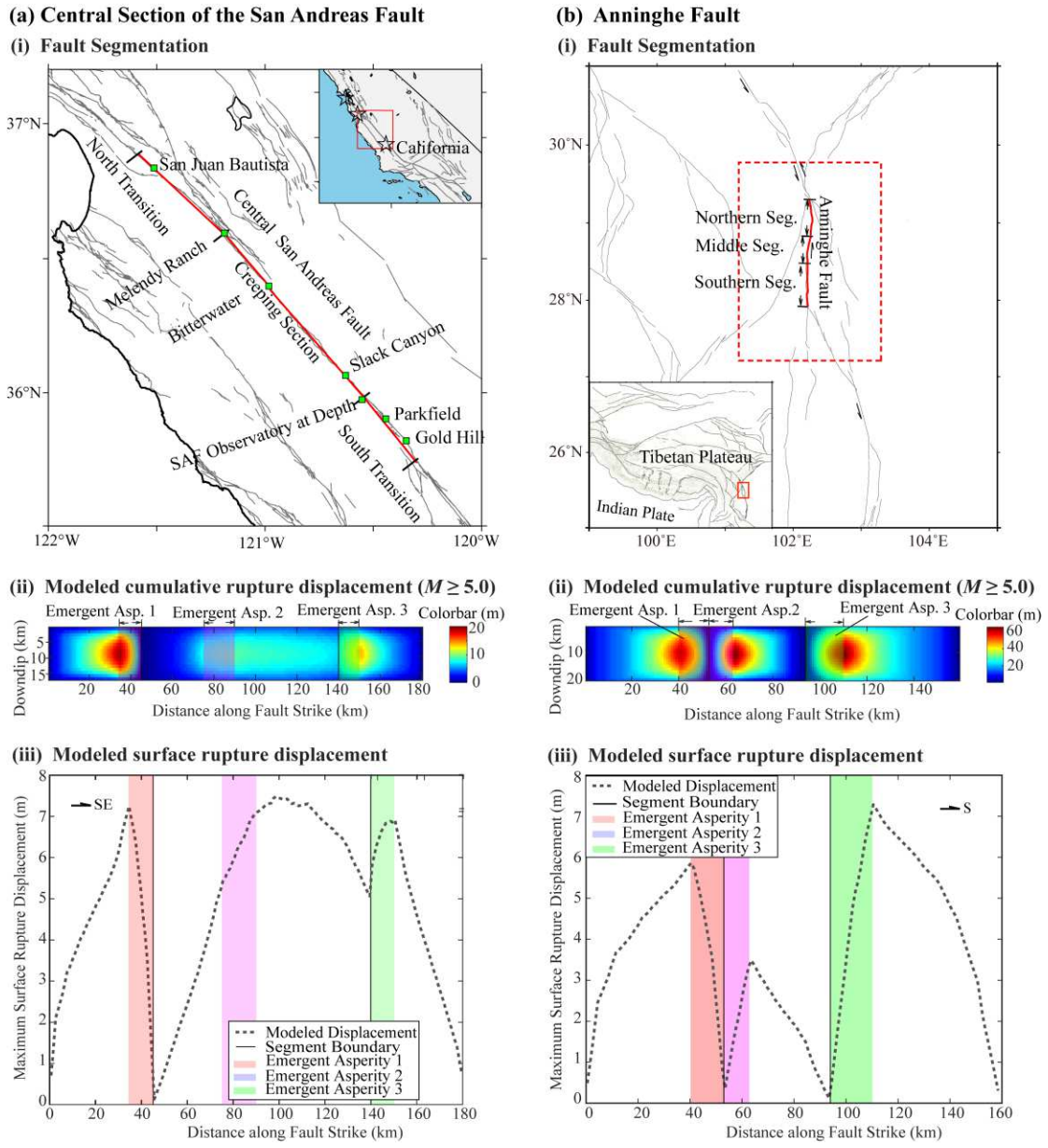


Figure 4 | Physics-based prediction of surface rupture displacement on segmented active faults. **a,b,** Application of the physics-based rupture displacement model to two representative segmented strike-slip fault systems: **(a)** the central section of the San Andreas Fault, USA, and **(b)** the Anninghe Fault, China. **(i)** Geological fault segmentation used in the forward simulations. Fault segments are defined from mapped active fault structures and geometric discontinuities, providing the finite fault framework for rupture scenarios. **(ii)** Predicted cumulative rupture displacement distributions along the segmented fault systems. Localized high-slip domains emerge from the interaction between rupture scaling, seismic moment conservation, and fault segmentation. These localized regions correspond to modeled asperity domains without prescribing spatial slip maxima or heterogeneous frictional patches. **(iii)** Predicted surface rupture displacement profiles along strike. The model captures strong along-strike variability in displacement amplitude, with peak displacements concentrated within emergent localized slip domains. Shaded regions indicate the modeled asperity domains, and vertical lines denote segment boundaries. These results demonstrate that

fault-specific surface rupture displacement can be predicted from a unified physical framework linking fault geometry, seismic moment conservation, and emergent asperity localization, without requiring empirical calibration of displacement patterns.

Discussion

Emergent asperity localization as a consequence of seismic moment conservation

A long-standing question in earthquake physics is whether asperities represent intrinsic properties of fault systems or are simply convenient descriptions of spatially heterogeneous rupture[41-44]. Most previous rupture models prescribe asperities through heterogeneous initial stress, frictional strength, or target slip distributions, thereby treating localized slip as an input rather than an outcome of the rupture process[7,42]. In contrast, our results suggest that localized slip concentrations can arise naturally from the combined effects of seismic moment conservation, finite fault geometry, and rupture scaling, without specifying asperity locations a priori.

Within the proposed framework, the total seismic moment accumulated during the seismic cycle is fixed by long-term tectonic loading, while rupture dimensions are constrained by fault geometry and earthquake magnitude[5,21]. Under these global constraints, homogeneous slip represents only one admissible configuration and is not the energetically preferred state of the constrained system. Small perturbations can evolve toward localized slip distributions while conserving the total moment, providing a simple physical explanation for the recurrent appearance of asperity-like structures on segmented strike-slip faults. The variational formulation presented in Figure 2 should therefore be interpreted as a reduced-order demonstration of localization instability under a fixed moment budget, rather than as a complete dynamic rupture simulation.

This perspective shifts the interpretation of asperities from prescribed structural entities to emergent properties of finite fault systems. Although natural faults undoubtedly contain structural and frictional heterogeneity[42], our results indicate that localized rupture does not necessarily require such heterogeneity to be explicitly imposed in predictive models.

A unified framework linking earthquake recurrence and surface rupture

An important feature of the present model is that earthquake occurrence and surface rupture displacement are derived within the same moment-balanced framework. Existing displacement prediction methods are commonly based on empirical regressions between earthquake magnitude and observed displacement or on stochastic

rupture realizations calibrated using historical earthquakes[2,5]. While these approaches have proved valuable for probabilistic hazard assessment, they generally provide limited insight into the physical origin of rupture variability.

Here, the earthquake recurrence model, rupture scaling relationship, and cumulative displacement calculation are linked through conservation of tectonic moment[5,21]. Consequently, the spatial distribution of rupture displacement is determined by the interaction between finite fault geometry and earthquake occurrence over multiple seismic cycles, rather than by event-specific calibration. This unified formulation explains why localized displacement repeatedly develops within particular portions of segmented faults and why different fault systems exhibit distinct rupture patterns despite similar regional tectonic loading conditions.

The successful reproduction of displacement variability across 23 historical strike-slip earthquakes further suggests that the principal controls on fault-scale rupture complexity can be captured using measurable geological parameters, including fault length, segmentation geometry, slip rate, and rupture scaling[5].

Implications for fault-specific seismic hazard assessment

Surface rupture hazard has become an increasingly important consideration in the design of critical infrastructure, including pipelines, transportation corridors, nuclear facilities, and lifeline systems[2]. Existing engineering practice typically relies on empirical displacement scaling relationships or deterministic scenario earthquakes, which often provide limited information regarding the spatial variability of future rupture along individual faults[2,5].

The present framework offers an alternative approach in which fault-specific displacement distributions are predicted directly from geological observations and long-term tectonic loading. Because the model does not require prior knowledge of future asperity locations, it can be applied to active faults for which no large historical earthquakes have been recorded. The forward simulations for the central San Andreas Fault and the Anninghe Fault demonstrate how cumulative rupture displacement may be estimated using only mapped fault geometry, slip rate, and earthquake recurrence statistics.

More broadly, the proposed framework provides a physically interpretable basis for incorporating surface rupture displacement into probabilistic fault-specific seismic hazard assessment. The methodology may therefore complement existing probabilistic

seismic hazard analysis by explicitly considering the spatial variability of future fault displacement[2].

Relationship to dynamic rupture models

The proposed framework is not intended to replace dynamic rupture simulations based on elastodynamic equations and constitutive friction laws. Dynamic rupture models remain indispensable for investigating rupture velocity, stress transfer, radiated seismic waves, and near-field ground motion[45-46]. However, these models generally require detailed knowledge of initial stress distributions, frictional properties, and constitutive parameters that are difficult to constrain for natural faults[42,46].

Instead, our approach addresses a different question: whether the large-scale organization of rupture displacement can be explained from global physical constraints without prescribing detailed fault heterogeneity. The variational localization model serves as a conceptual demonstration showing that localized slip represents an energetically preferred configuration under a fixed seismic moment constraint. The subsequent rupture simulations then translate this physical principle into fault-scale displacement predictions using observed fault geometry and earthquake recurrence statistics.

Accordingly, the two approaches should be regarded as complementary rather than competing. Reduced-order models based on conservation principles may provide physically constrained initial conditions or long-term boundary conditions for future dynamic rupture simulations, while fully dynamic models can further investigate the short-timescale processes governing rupture propagation within the localized slip regions predicted by the present framework[46].

Limitations and future developments

Several limitations should be acknowledged. First, the current model assumes uniform elastic properties and does not explicitly represent spatial variations in lithology, stress field, or frictional strength. Consequently, local displacement anomalies associated with secondary faulting, shallow sediment deformation, or off-fault damage are not reproduced[47-49].

Second, the variational formulation is introduced solely to demonstrate the physical mechanism underlying localization instability and is not intended to represent the complete elastodynamic evolution of earthquake rupture. The predicted localized slip domains therefore represent the first-order spatial organization of rupture rather than detailed coseismic slip distributions for individual earthquakes.

Finally, the present study focuses exclusively on segmented strike-slip faults. Extension of the framework to normal and thrust fault systems, incorporation of time-dependent stress evolution, and coupling with dynamic rupture simulations represent promising directions for future research. Integrating geological observations, geodetic measurements, and physics-based rupture models within the same moment-constrained framework may ultimately improve fault-specific forecasts of future earthquake rupture and associated seismic hazards.

Methods

Overview of the modeling framework

The proposed framework predicts fault-scale surface rupture displacement by integrating long-term tectonic loading, earthquake recurrence, rupture geometry, and cumulative coseismic deformation within a unified moment-constrained formulation. Rather than prescribing asperity locations or heterogeneous frictional properties, localized slip distributions emerge from the interaction between finite fault geometry and the cumulative seismic moment budget over multiple earthquake cycles.

The complete workflow consists of five sequential components (Fig. 1): (1) construction of a segmented fault model from mapped fault geometry; (2) calculation of earthquake occurrence rates using a moment-balanced truncated Gutenberg–Richter relationship[21]; (3) estimation of rupture dimensions through magnitude-dependent scaling laws[20,23]; (4) stochastic simulation of earthquake ruptures over repeated seismic cycles; and (5) accumulation of rupture displacement to obtain fault-scale displacement distributions. A reduced-order variational model is further introduced to illustrate the physical origin of slip localization under a fixed seismic moment constraint (Fig. 2). The variational model serves only as a conceptual demonstration of localization instability and is not intended to simulate the complete elastodynamic rupture process.

Fault geometry and discretization

Each fault is represented as a finite rectangular rupture surface characterized by fault length L, downdip width W, and long-term slip rate V_S. The fault plane is discretized into uniform square cells with grid size Δx, allowing rupture occurrence and cumulative displacement to be evaluated on individual subfaults. The discretized fault

contains $N_x = \frac{L}{\Delta x}$, $N_y = \frac{L}{\Delta y}$, grid cells along strike and dip directions, respectively. Each grid cell represents an elemental rupture area $A_i = \Delta x^2$.

Fault segmentation is defined directly from geological mapping. Segment boundaries constrain rupture propagation by limiting the spatial extent of possible earthquake ruptures[1]. No asperity locations are specified during fault construction.

For the applications presented here, mapped fault geometries of the central San Andreas Fault[24,25] and the Anninghe Fault[26,27] were adopted from published geological datasets. Historical earthquake ruptures were reconstructed using reported rupture traces and rupture dimensions compiled from field observations and remote sensing (Supplementary Table S4).

Moment-balanced earthquake occurrence model

Earthquake occurrence is described using a truncated Gutenberg–Richter frequency–magnitude relationship constrained by the long-term tectonic moment rate[21]. The cumulative annual occurrence rate for earthquakes with magnitude greater than or equal to M is

$$N(M) = 10^{a-bM} \tag{4}$$

where b is the Gutenberg–Richter parameter.

Unlike conventional recurrence models in which the normalization constant is obtained empirically, the present model determines earthquake occurrence by enforcing conservation of tectonic moment. The cumulative seismic moment released during the complete seismic cycle satisfies

$$\sum_k M_{0,k} N_k = \dot{M}_{tectonic} \tag{5}$$

where

$$\dot{M}_{tectonic} = \mu L W V_s \tag{6}$$

is the long-term tectonic moment accumulation rate, μ is the shear modulus, and V_S is the geological slip rate.

The largest earthquake magnitude is determined by the finite dimensions of the mapped fault rather than treated as an adjustable parameter. Consequently, earthquake recurrence, maximum magnitude, and tectonic loading are internally consistent within a single moment-balanced framework[5,21].

Magnitude-dependent rupture scaling

For each simulated earthquake magnitude, rupture dimensions are estimated using empirical rupture-scaling relationships.

Following Leonard (2014)[20],

$$\log L_r = a - bM_w \tag{7}$$

where L_r denotes rupture length.

For earthquakes whose rupture width is controlled by the seismogenic thickness, rupture width is fixed by the mapped fault geometry. Smaller events employ magnitude-dependent rupture width scaling[20,23].

The seismic moment for each event is

$$M_0 = 10^{1.5M_w+9.05} \tag{8}$$

and the average rupture slip becomes

$$D = \frac{M_0}{\mu L_r W_r} \tag{9}$$

These relationships determine rupture size and average slip for every earthquake generated within the recurrence model[20,23].

Monte Carlo rupture simulation

Earthquake ruptures are simulated using stochastic sampling along the discretized fault plane.

For every magnitude interval, rupture occurrence frequency is obtained from the truncated Gutenberg–Richter model. Rupture nucleation locations are then sampled randomly within the fault while satisfying geometric constraints on rupture dimensions.

Each simulated rupture contributes

$$\Delta D = D\frac{N(M)}{N_{sample}} \tag{10}$$

to every intersected sub-fault, where N_{sample} denotes the number of Monte Carlo realizations used for numerical integration.

Repeated rupture simulations over the complete magnitude range produce cumulative rupture participation for each sub-fault, yielding spatial distributions of earthquake occurrence and cumulative displacement over the seismic cycle.

Because rupture positions are randomly sampled without specifying preferred nucleation sites or slip maxima, any spatial concentration of displacement arises solely from finite fault geometry, rupture overlap, and conservation of tectonic moment.

Surface rupture displacement estimation

Cumulative fault displacement is calculated by summing the coseismic contribution from all simulated earthquakes intersecting each grid cell,

$$D_{cum}(i) = \sum_{k} D_k(i) \tag{11}$$

where $D_k(i)$ is the displacement contribution from earthquake k.

To estimate observable surface displacement, cumulative displacement is projected to the shallow fault surface using an exponential attenuation function,

$$D_{surface} = D_{surface}\exp(-\frac{h}{R}) \tag{12}$$

where h denotes the effective thickness of the shallow compliant layer and R is the characteristic attenuation length.

The attenuation function accounts for distributed deformation within near-surface sediments and weathered rocks while preserving the along-strike displacement pattern predicted by the fault model[11,36,48].

Numerical demonstration of slip localization

To illustrate the physical mechanism responsible for localized rupture development, we introduce a reduced-order variational model in which the slip distribution evolves under the constraint of fixed seismic moment.

The total moment satisfies

$$M_0 = \sum_{i} \mu A_i D_i \tag{13}$$

The numerical experiment begins from an approximately uniform slip distribution with small random perturbations while preserving the total seismic moment.

At each iteration, local slip values are adjusted according to a gradient-based relaxation scheme, after which the slip field is renormalized to satisfy the prescribed moment constraint. The procedure progressively redistributes slip while maintaining constant total seismic moment.

The resulting evolution demonstrates that homogeneous slip represents an unstable configuration under the constrained optimization, whereas localized slip domains correspond to energetically preferred states. Importantly, no asperity locations, heterogeneous frictional patches, or prescribed slip concentrations are introduced during the calculation. The variational demonstration therefore illustrates only the physical origin of localization instability and should not be interpreted as a dynamic rupture simulation[45].

Additional mathematical formulation, numerical implementation, and convergence analyses are presented in Supplementary Note S2.

Model validation and predictive applications

The proposed framework was evaluated using two complementary approaches.

First, retrospective validation was performed using 23 historical strike-slip earthquakes spanning a broad range of rupture lengths, magnitudes, and tectonic environments. Published geological field measurements, InSAR observations, and high-resolution remote-sensing interpretations were compiled to compare modeled and observed surface displacement distributions (Supplementary Tables S2–S4).

Second, prospective simulations were conducted for the central San Andreas Fault and the Anninghe Fault using only mapped fault geometry, geological slip rate, and recurrence statistics. No earthquake-specific displacement observations or asperity locations were incorporated into these simulations. The resulting displacement distributions therefore represent genuine forward predictions derived from the physical framework.

References and Notes

1. Wesnousky, S. G. Displacement and geometrical characteristics of earthquake surface ruptures. BSSA, 98, 1609–1632 (2008).
2. Petersen, M. D. et al. Fault displacement hazard for strike-slip faults. *Bull. Seismol. Soc. Am.* **101**, 805–825 (2011).
3. Segall, P. & Pollard, D. Mechanics of discontinuous faults. *J. Geophys. Res.: Solid Earth* **85**, 4337–4350 (1980).
4. Segall, P. Integrating geologic and geodetic estimates of slip rate on the San Andreas fault system. *International Geology Review* **44**, 62–82 (2002).

5. Wells, D. L. & Coppersmith, K. J. New empirical relationships among magnitude, rupture length, rupture width, rupture area, and surface displacement. *Bull. Seismol. Soc. Am.* **84**, 974–1002 (1994).
6. Shaw, B. E. & Wesnousky S. G. Slip-length scaling in large earthquakes: The role of deep-penetrating slip below the seismogenic layer. *Bull. Seismol. Soc. Am.* **98**, 1633–1641 (2008).
7. Lay, T. & Kanamori, H. An asperity model of large earthquake sequences. *Earthquake Predict.* **4**, 579–592 (1981).
8. Johnson, L. R. & Nadeau, M. Asperity model of an earthquake: Static problem. *Bull. Seismol. Soc. Am.* **92**, 672–686 (2002).
9. Murotani, S., Satake, K. & Fujii, Y. Scaling relations of seismic moment, rupture area, average slip, and asperity size for M ∼ 9 subduction-zone earthquakes. *Geophys. Res. Lett.* **40** (19), 5070–5074 (2013).
10. Venegas-Aravena, P., Crempien, J. & Archuleta, R. Fractal spatial distributions of initial shear stress and frictional properties on faults and their impact on dynamic earthquake rupture. *Bull. Seism. Soc. Am.* **114** (3), 1444–1465 (2024).
11. Dalguer, L. A., Miyake, H., Day, S. M., & Irikura, K. Surface rupturing and buried dynamic-rupture models calibrated with statistical observations of past earthquakes. *Bull. Seismol. Soc. Am.* **98**, 1147–1161 (2008).
12. Bruhat, L., Klinger, Y., Vallage, A. & Dunham, E. Influence of fault roughness on surface displacement: From numerical simulations to coseismic slip distributions. *Geophys. J. Int.* **220**, 1857–1877 (2020).
13. Cattania, C. & Segall, P. Precursory Slow Slip and Foreshocks on Rough Faults. *J. Geophys. Res.: Solid Earth* **126**, e2020JB020430 (2021)
14. Scholz, C. H. *The mechanics of earthquakes and faulting*. Cambridge University Press, New York (2018).
15. Bürgmann, R. et al. Interseismic coupling and asperity distribution along the Kamchatka subduction zone. *J. Geophys. Res.* **110**, B07405 (2005).
16. Seno, T. Fractal asperities, invasion of barriers, and interplate earthquakes. *Earth Planets Space* **55**, 649–665 (2003).
17. Wang, L., Xu, S., Zhuo, Y., Liu, P. & Ma, S. Unraveling the roles of fault asperities over earthquake cycles. *Earth Planet. Sci. Lett.* **636**, 15, 118711 (2024).

18. Scholz, C., Aviles, C. & Wesnousky, S. Scaling differences between large interplate and intraplate earthquakes. *Bull. Seismol. Soc. Am.* **76**, 65–70 (1986).
19. Johnson, K. M., Mavrommatis, A., & Segall, P. Small interseismic asperities and widespread aseismic creep on the northern Japan subduction interface. *Geophys. Res. Lett.* **43**, 135–143 (2010).
20. Leonard, M. Self-consistent earthquake fault scaling relations. *Bull. Seismol. Soc. Am.* **104**, 2953–2965 (2014).
21. Youngs, R. R. & Coppersmith, K. J. Implications of fault slip rates and earthquake recurrence models to probabilistic seismic hazard estimates. *Bull. Seismol. Soc. Am.* **75**, 939–964 (1985).
22. Furlong, K. "The Intraplate Earthquake Cycle: Strain and Displacement Behavior During the Canterbury, New Zealand, Earthquake Sequence" (NEHRP Tech. Rep. G12AP20031, 2012).23 (2012).
23. Cheng, J. et al. Earthquake rupture scaling relations for mainland China. *Seismol. Res. Lett.* **91**, 248–261 (2020).
24. Cheng, Y., Bürgmann, R. & Allen, R. 3D architecture and complex behavior along the simple central San Andreas fault. *Nat. Commun.* **15**, 49454 (2024).
25. Liu, Y., Ross, Z., Cochran, E. & Lapusta N. A unified perspective of seismicity and fault coupling along the San Andreas Fault. *Sci. Adv.* **8**, eabk1167 (2022).
26. Jiang, G. et al. Geodetic imaging of potential seismogenic asperities on the Xianshuihe-Anninghe-Zemuhe fault system, southwest China, with a new 3D viscoelastic interseismic coupling model. *J. Geophys. Res.* **120**, 1855–1873 (2015).
27. Cheng, J. et al. Seismic hazard of multi-segment rupturing for the Anninghe–Zemuhe–Daliangshan fault region, southeastern Tibetan Plateau: constraints from geological and geodetic slip rates. *Nat. Hazards* **107**, 1501–1525 (2021).
28. Sieh, K. Slip along the San Andreas Fault associated with the great 1857 earthquake. *Bull. Seismol. Soc. Am.* **68**, 1421–1448 (1978).
29. Zielke, J., Arrowsmith, J. R., Ludwig, L. G. & Akciz, S. Slip in the 1857 and earlier large earthquakes along the Carrizo Plain, San Andreas Fault. *Science* **327**, 1119–1122 (2010).

30. Lasserre, C. et al. Coseismic deformation of the 2001 Mw 7.8 Kokoxili earthquake in Tibet, measured by synthetic aperture radar interferometry. *J. Geophys. Res.* **110**, B12408 (2005).
31. Ren, J. et al. Coseismic surface ruptures, slip distribution, and 3D seismogenic fault for the 2021 *M*w7.3 Maduo earthquake, central Tibetan Plateau, and its tectonic implications. *Tectonophysics* **827**, 229275 (2022).
32. Liu-Zeng, J. et al. Fault orientation trumps fault maturity in controlling coseismic rupture characteristics of the 2021 Maduo earthquake. *AGU Adv.* **5**, e2023AV001134 (2024).
33. Yue, H. et al. Rupture process of the 2021 M7.4 Maduo earthquake and implication for deformation mode of the Songpan-Ganzi terrane in Tibetan Plateau. *Proc. Natl. Acad. Sci. USA* **119**, e2116445119 (2022).
34. Ren, C. et al. Supershear triggering and cascading fault ruptures of the 2023 Kahramanmaraş, Türkiye, earthquake doublet. *Science* **383**, 305–311 (2024).
35. Meng, J. Surface deformations of the 6 February 2023 earthquake sequence, eastern Türkiye. *Science* **383**, 298–305 (2024).
36. Vavra, E. et al. The 2023 Mw 7.8–7.7 Kahramanmaraş earthquakes were loosely slip-predictable. *Commun. Earth Environ.* **6**, 80 (2025). https://doi.org/10.1038/s43247-024-01969-5
37. Antoine, S. L. et al. The 2025 *M*w 7.7 Mandalay, Myanmar, earthquake reveals a complex earthquake cycle with clustering and variable segmentation on the Sagaing Fault. *Proc. Natl. Acad. Sci. U.S.A.* **122**, e2514378122 (2025).
38. Klinger, Y., Michel, R. & King, G. Evidence for an earthquake barrier model from Mw ~7.8 Kokoxili (Tibet) earthquake slip distribution. *Earth Planet. Sci. Lett.* **242**, 354–364 (2006).
39. Ye, L., Lay, T. & Kanamori, H. The 28 March 2025 Mw 7.8 Myanmar earthquake: preliminary analysis of an ~480 km long intermittent supershear rupture. *Seism. Rec.* **5** (3), 260–269 (2025).
40. Cohee, B. & Beroza, G. C. Slip distribution of the 1992 Landers earthquake and its implications for earthquake source mechanics. *Bull. Seismol. Soc. Am.* **84**, 692–712 (1994).

41. Scholz, C. H. *The mechanics of earthquakes and faulting*. Cambridge University Press, New York (2018).
42. Mai, P. M. & Beroza, G. C. A spatial random field model to characterize complexity in earthquake slip. *J. Geophys. Res.* **107**, 2308 (2002).
43. Somerville, P. et al. Characterizing crustal earthquake slip models for the prediction of strong ground motion. *Seismol. Res. Lett.* **70**, 59–80 (1999).
44. Kanamori, H. & Stewart, G. S. Seismological aspects of the Guatemala earthquake of February 4, 1976. *J. Geophys. Res.* **83**, 3427–3434 (1978).
45. Andrews, D. J. Rupture velocity of plane strain shear cracks. *J. Geophys. Res.* **81**, 5679–5687 (1976).
46. Harris, R. A. & Day, S. M. Dynamic 3D simulations of earthquakes on en echelon faults. *Geophys. Res. Letts*. **26**, 2089-2092 (1999).
47. Barka, A. et al. The surface rupture and slip distribution of the 17 August 1999 Izmit earthquake (M 7.4), North Anatolian Fault. *Bull. Seismol. Soc. Am.* **92**, 43–60 (2002).
48. Milliner, C. et al. Quantifying near-field and off-fault deformation patterns of the 1992 Mw7.3 Landers earthquake. *Geochem. Geophys. Geosyst.* **16**, e2014GC005693 (2015).
49. Gold, R. et al. On- and off-fault deformation associated with the September 2013 Mw7.7 Balochistan earthquake: Implications for geologic slip rate measurements. *Tectonophysics* **660**, 65–78 (2015).

Acknowledgments

We thank Prof. Jie Liu from China Earthquake Networks Center for discussing of the earthquake rupture mechanisms. We are grateful to Junjie Ren from China University of Geosciences, Beijing and Xiaodong Song from Peking University for rupture parameters collection. We are also indebted to Dr. Yifang Cheng from Tongji University and Dr. Lingling Ye from the South China University of Science and Technology for their valuable discussions. This study was supported by the National Natural Science Foundation of China, 42474078 and 42074064, and Disciplinary Development Fund of China University of Geosciences, Beijing, 2023010.

Author contributions

J.C. conceived and designed the study. J.C. and X.X. developed the methodology and performed the simulations. J.C. analyzed the results. J.C. and X.X. wrote the original draft, and both authors reviewed and edited the manuscript.

Competing interests

The authors declare no competing interests.

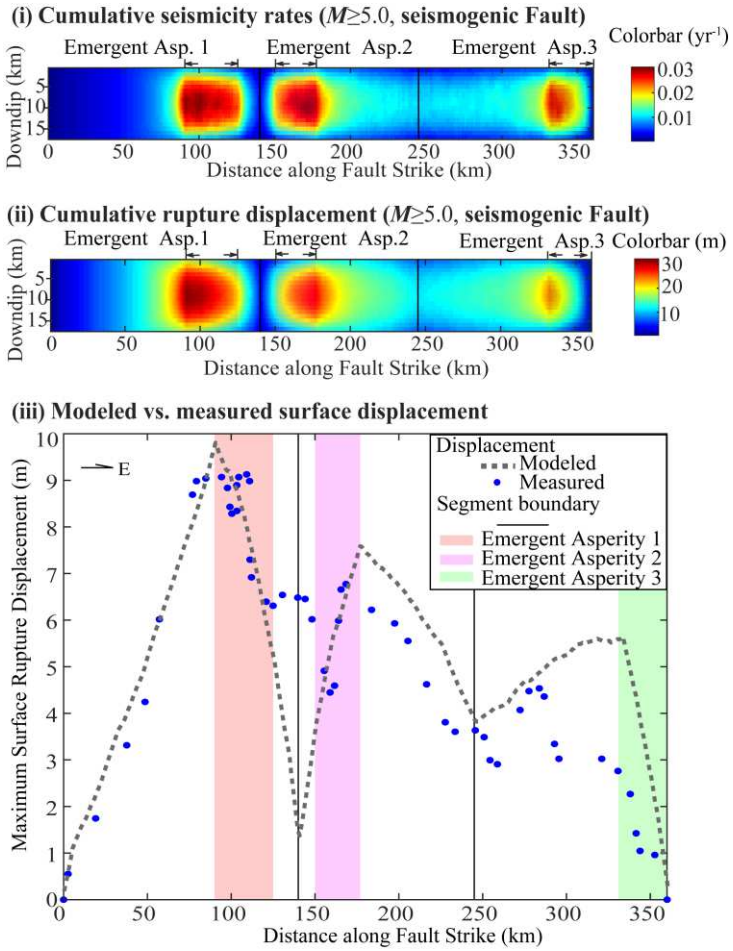
Additional information

Extended Data Fig. 1-Extended Data Fig. 19 are provided with this paper.

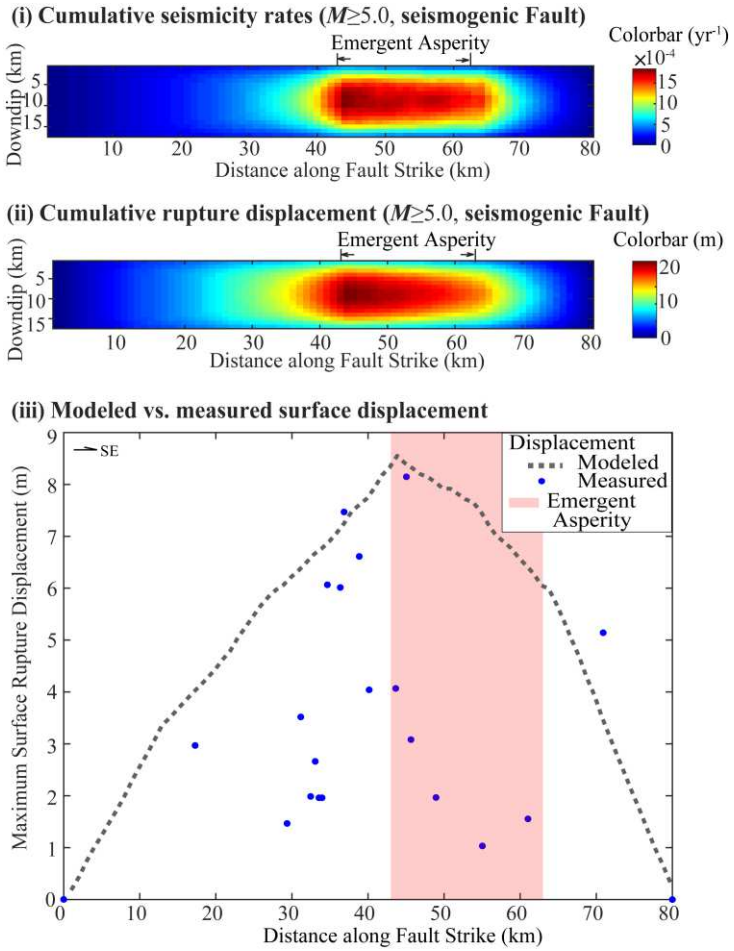
Supplementary information is available, including Supplementary Methods, Fig. S1, and Tables S1–S10. Surface rupture displacement data compiled from Wesnousky[1], and additional sources are summarized in Tables S4–S10.

Code availability

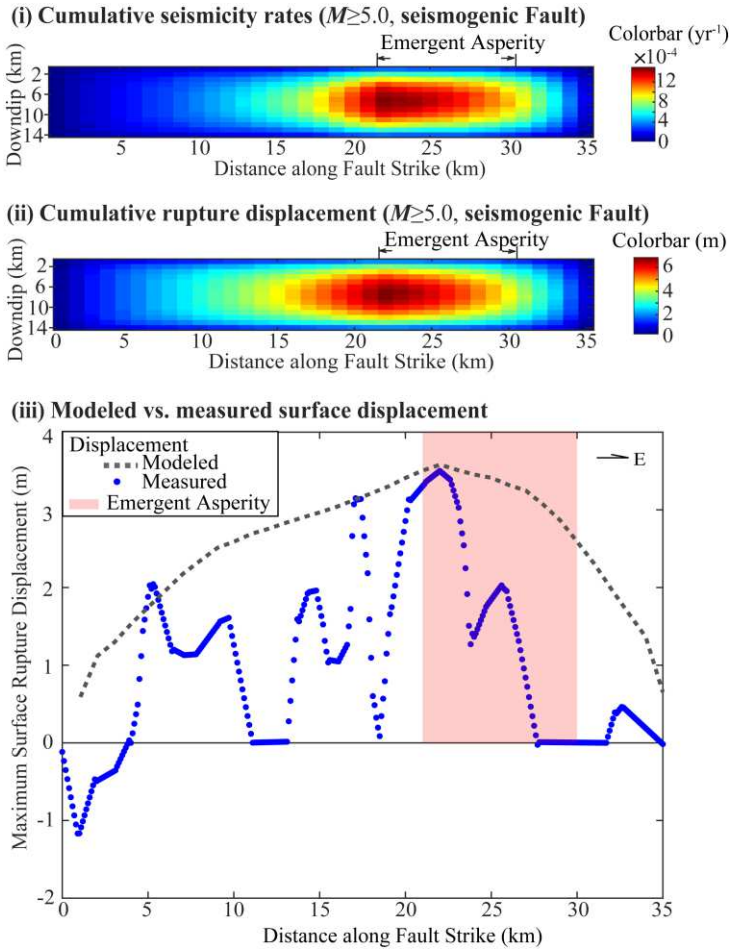
The source code of Coseismic Horizontal-slip Earth-surface Nonlinear Geosimulator are available at Code Ocean for review.



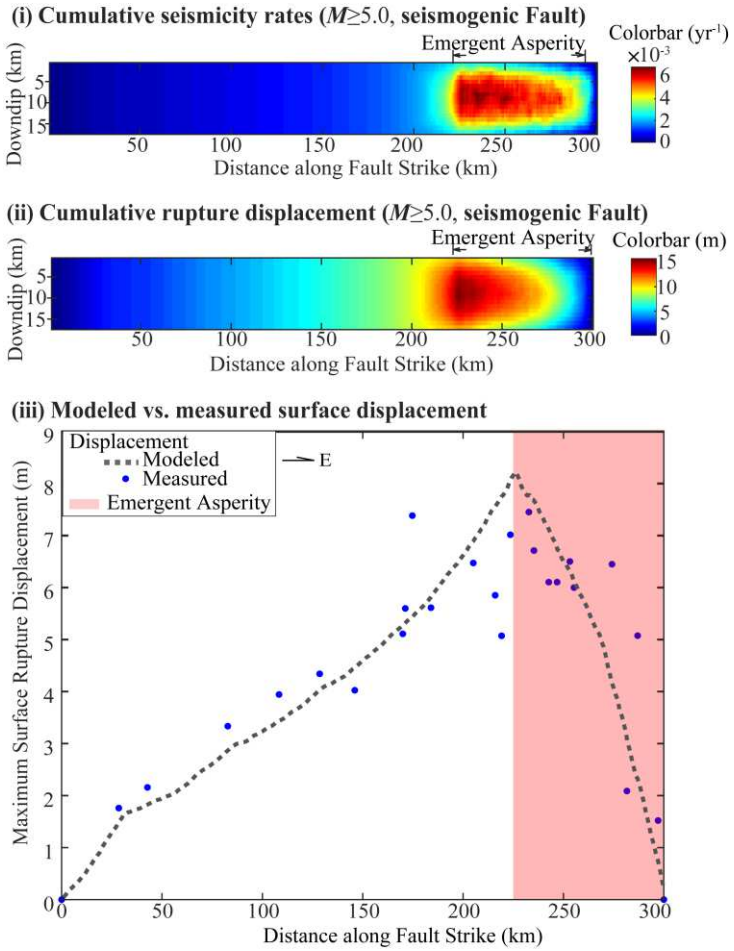
Extended Data Fig. 1 Asperity-controlled rupture and surface displacement for 1857 *M*w7.9 Fort Tejon Earthquake, USA. Panels show (i) modeled surface rupture displacement, (ii) corresponding fault-plane displacement prior to near-surface adjustment, and (iii) cumulative along-strike seismicity rate.



Extended Data Fig. 2 Asperity-controlled rupture and surface displacement for 1891 *M*w7.3 Nobi Earthquake, Japan. Panels show (i) modeled surface rupture displacement, (ii) corresponding fault-plane displacement prior to near-surface adjustment, and (iii) cumulative along-strike seismicity rate.



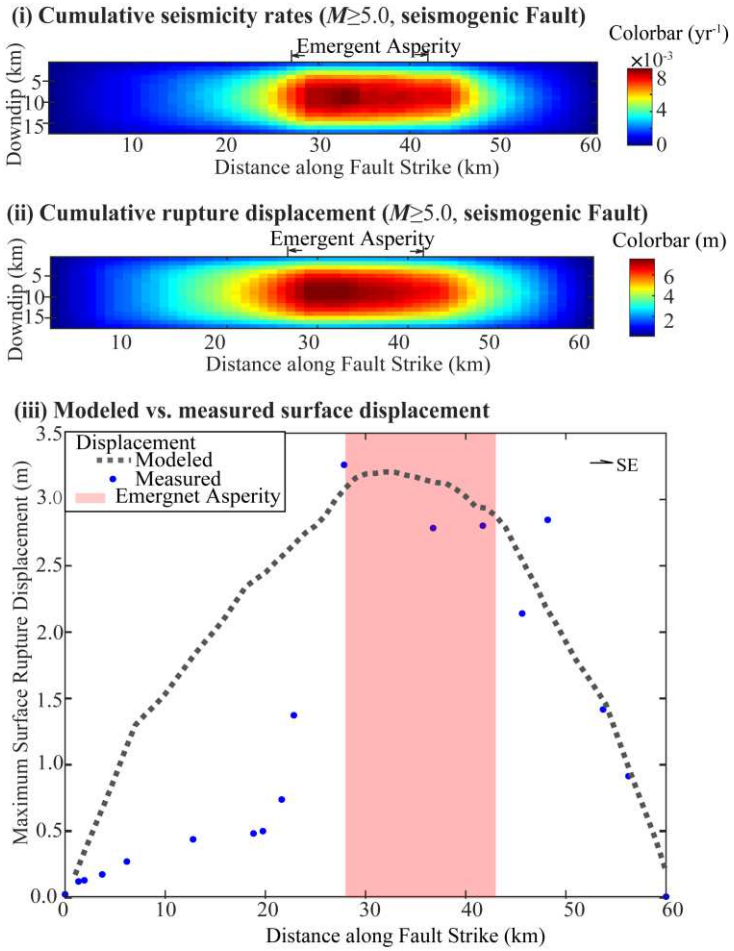
Extended Data Fig. 3 Asperity-controlled rupture and surface displacement for 1930 M_W6.7 Kita-Izu Earthquake, Japan. Panels show (i) modeled surface rupture displacement, (ii) corresponding fault-plane displacement prior to near-surface adjustment, and (iii) cumulative along-strike seismicity rate.



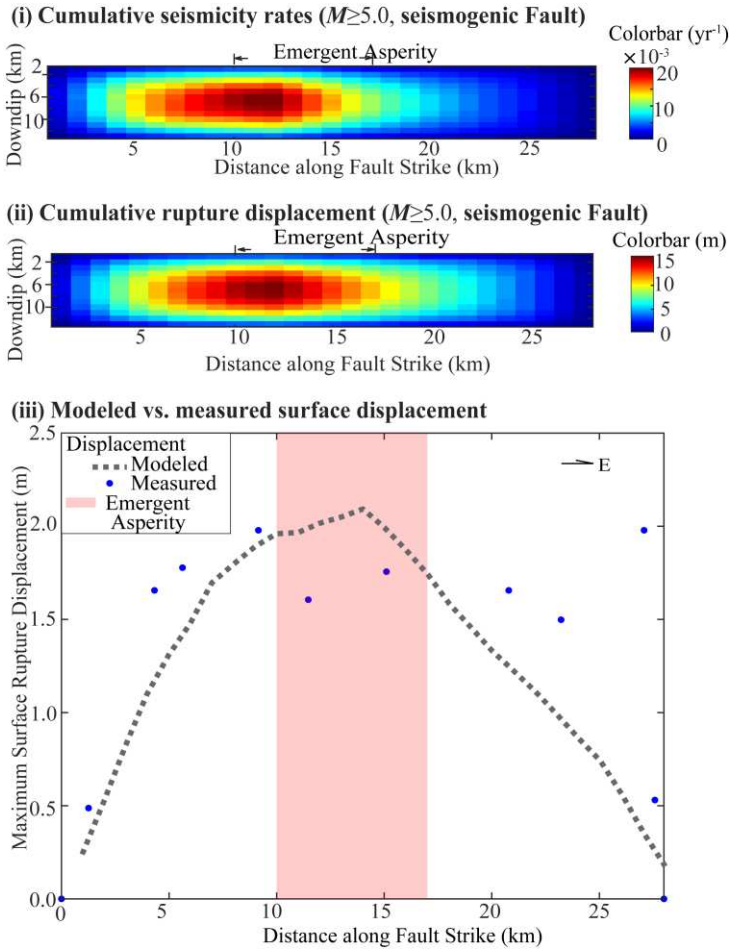
790

791 **Extended Data Fig. 4 Asperity-controlled rupture and surface displacement**
792 **for 1939 M_W7.7 Erzincan Earthquake, Türkiye.** Panels show (i) modeled surface
793 rupture displacement, (ii) corresponding fault-plane displacement prior to near-surface
794 adjustment, and (iii) cumulative along-strike seismicity rate.

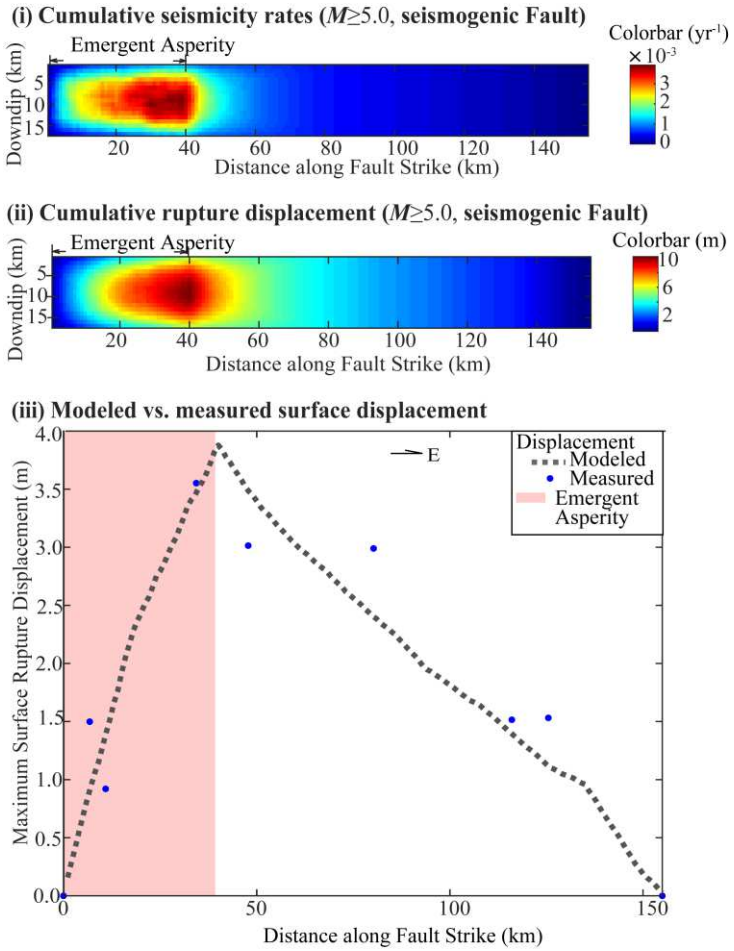
795



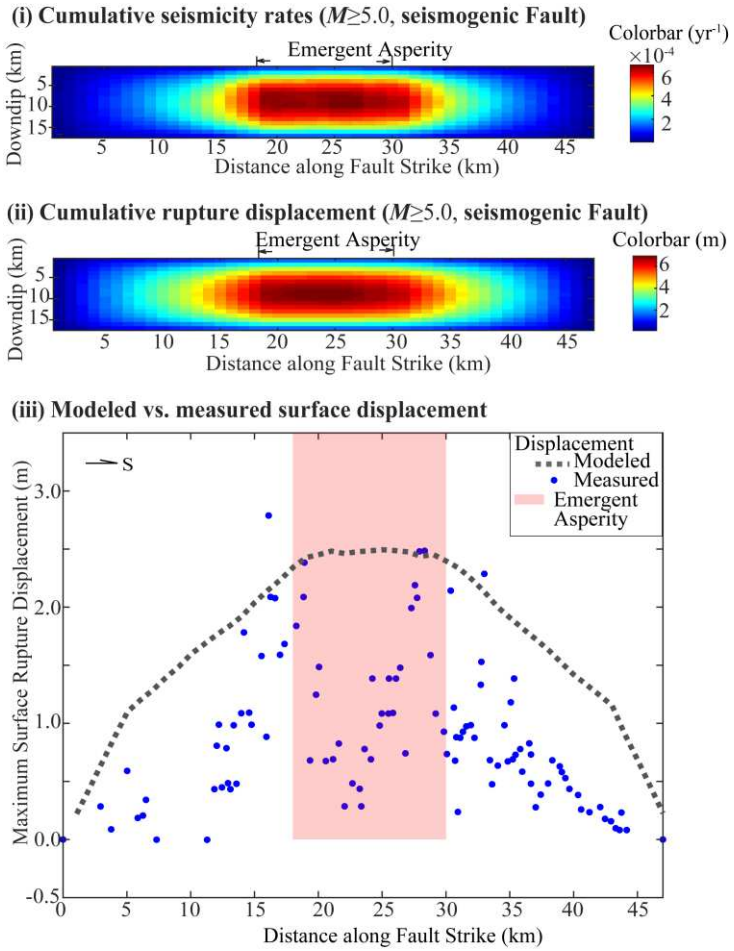
Extended Data Fig. 5 Asperity-controlled rupture and surface displacement for 1940 *M*w6.9 Imperial Earthquake, USA. Panels show (i) modeled surface rupture displacement, (ii) corresponding fault-plane displacement prior to near-surface adjustment, and (iii) cumulative along-strike seismicity rate.



Extended Data Fig. 6 Asperity-controlled rupture and surface displacement for 1942 M_W6.8 Erbaa-Niksar Earthquake, Türkiye. Panels show (i) modeled surface rupture displacement, (ii) corresponding fault-plane displacement prior to near-surface adjustment, and (iii) cumulative along-strike seismicity rate.



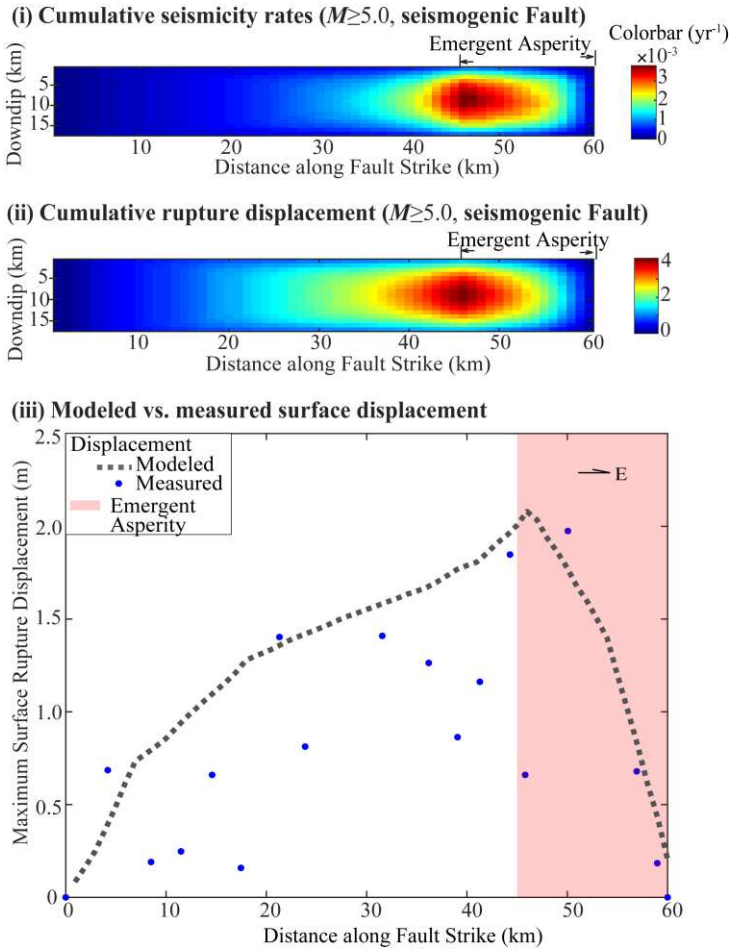
Extended Data Fig. 7 Asperity-controlled rupture and surface displacement for 1944 M_W7.35 Gereda-Bolu Earthquake, Türkiye. Panels show (i) modeled surface rupture displacement, (ii) corresponding fault-plane displacement prior to near-surface adjustment, and (iii) cumulative along-strike seismicity rate.



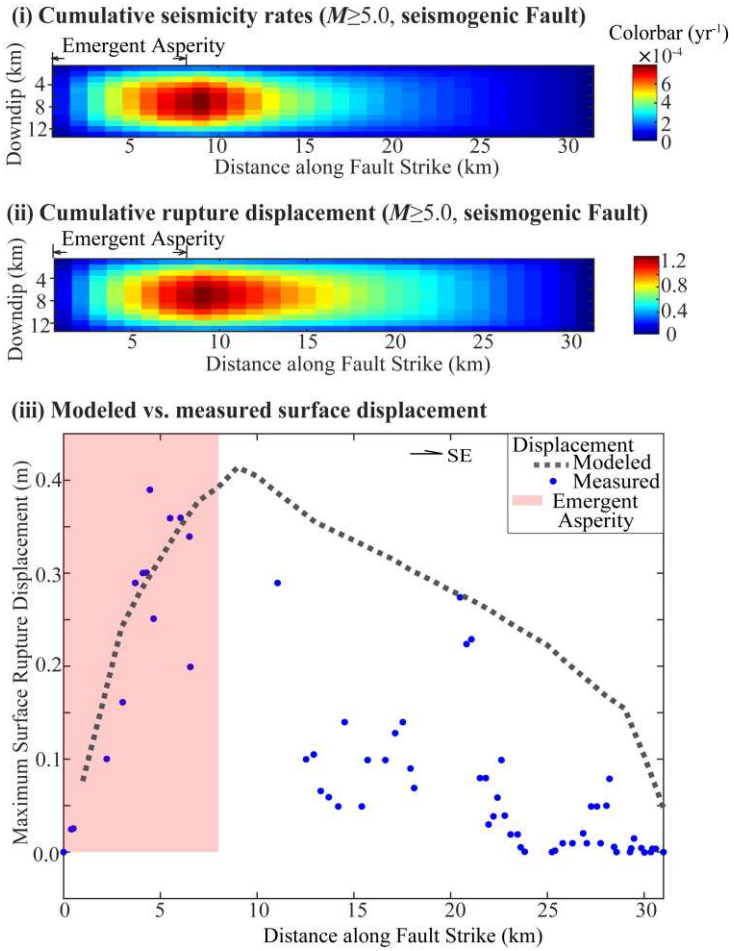
814

815 **Extended Data Fig. 8 Asperity-controlled rupture and surface displacement**
816 **for 1954 M_W6.8 Dixie Valley Earthquake, USA.** Panels show (i) modeled surface
817 rupture displacement, (ii) corresponding fault-plane displacement prior to near-surface
818 adjustment, and (iii) cumulative along-strike seismicity rate.

819



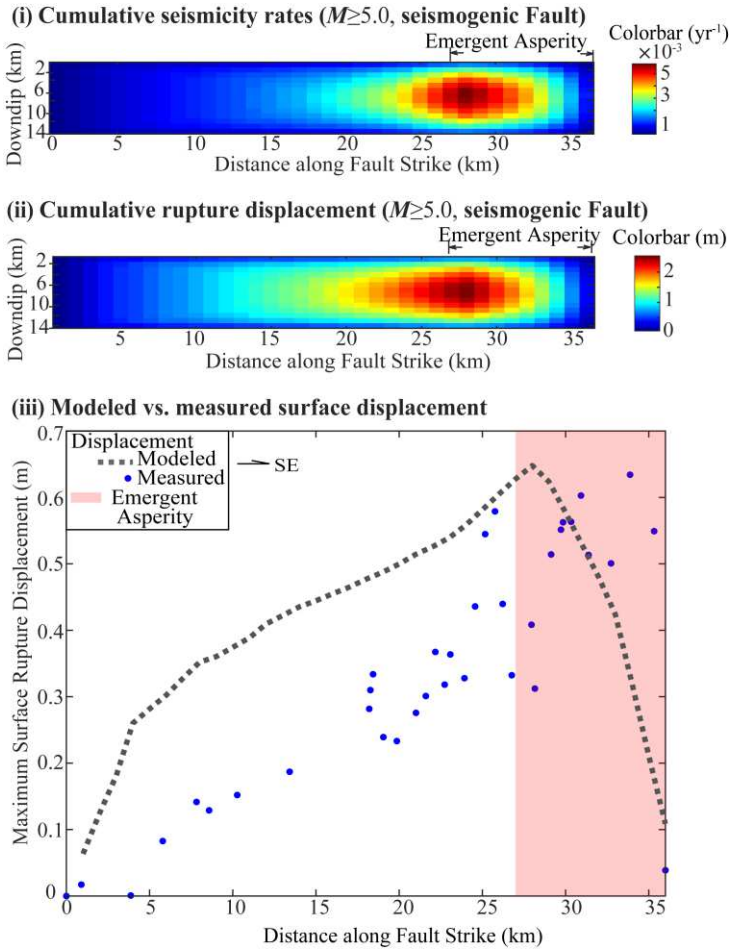
Extended Data Fig. 9 Asperity-controlled rupture and surface displacement for 1967 *M*w6.7 Mudurnu Earthquake, Türkiye. Panels show (i) modeled surface rupture displacement, (ii) corresponding fault-plane displacement prior to near-surface adjustment, and (iii) cumulative along-strike seismicity rate.



826

827 **Extended Data Fig. 10 Asperity-controlled rupture and surface displacement**
828 **for 1968 *M*w6.1 Borrego Earthquake, USA.** Panels show (i) modeled surface rupture
829 displacement, (ii) corresponding fault-plane displacement prior to near-surface
830 adjustment, and (iii) cumulative along-strike seismicity rate.

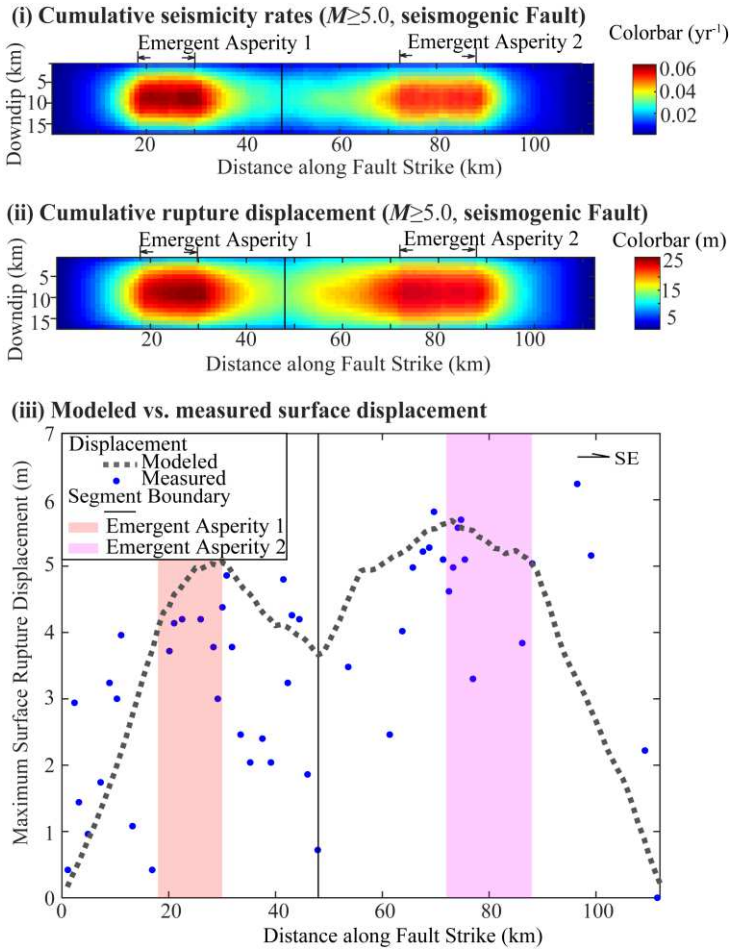
831



832

833 **Extended Data Fig. 11 Asperity-controlled rupture and surface displacement**
834 **for 1979 *M*w6.4 Imperial Valley Earthquake, USA.** Panels show (i) modeled surface
835 rupture displacement, (ii) corresponding fault-plane displacement prior to near-surface
836 adjustment, and (iii) cumulative along-strike seismicity rate.

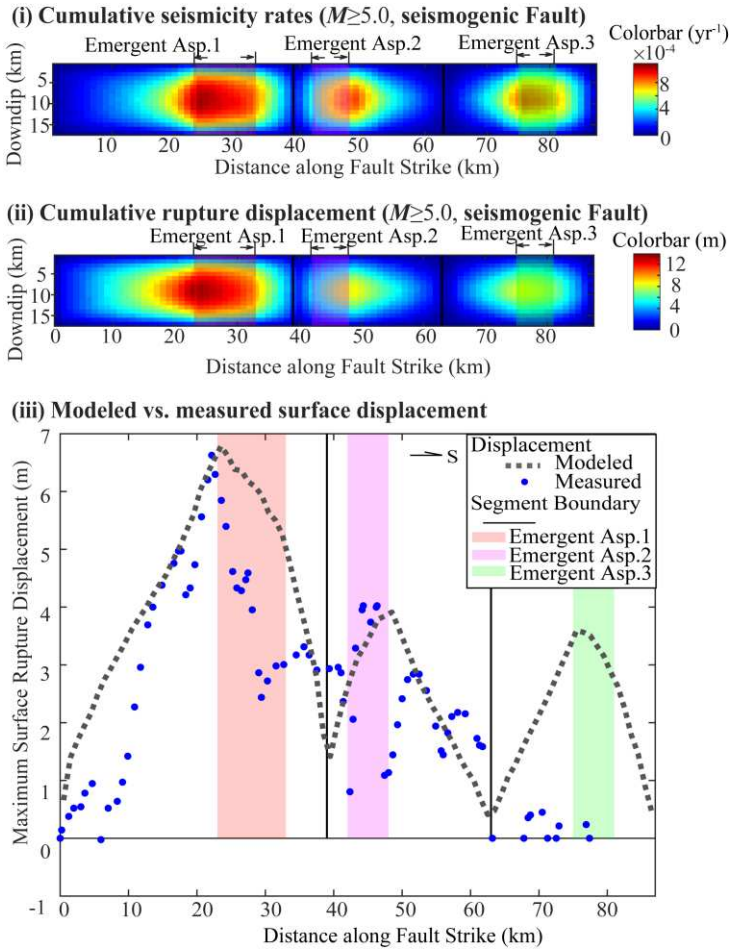
837



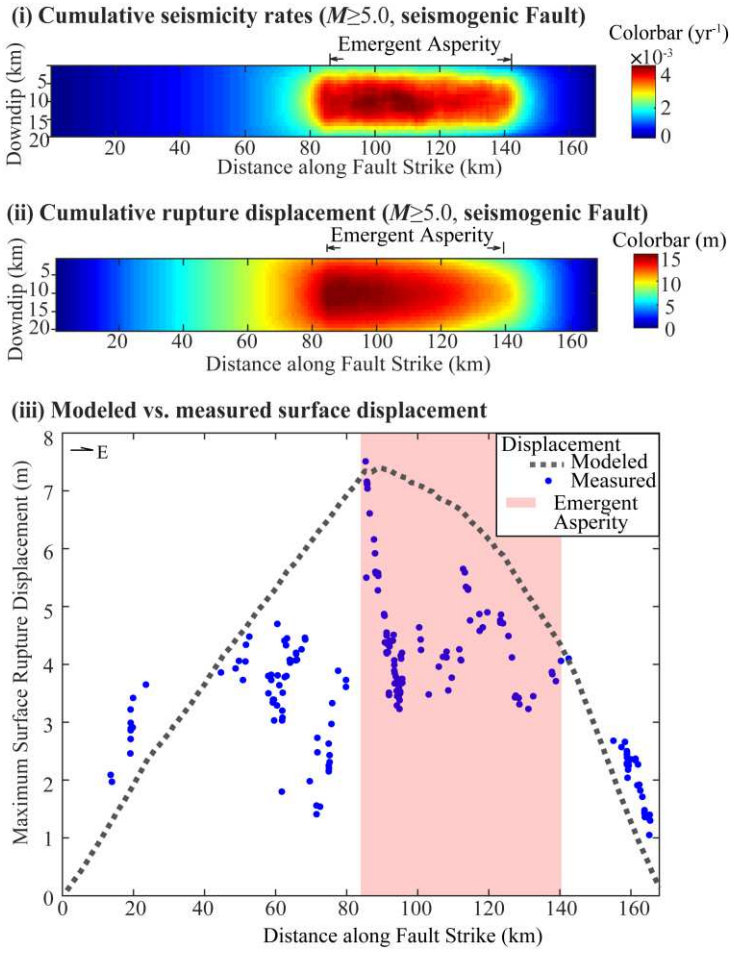
838

839 **Extended Data Fig. 12 Asperity-controlled rupture and surface displacement**
840 **for 1990 *M*w7.6 Luzon Earthquake, Philippines.** Panels show (i) modeled surface
841 rupture displacement, (ii) corresponding fault-plane displacement prior to near-surface
842 adjustment, and (iii) cumulative along-strike seismicity rate.

843



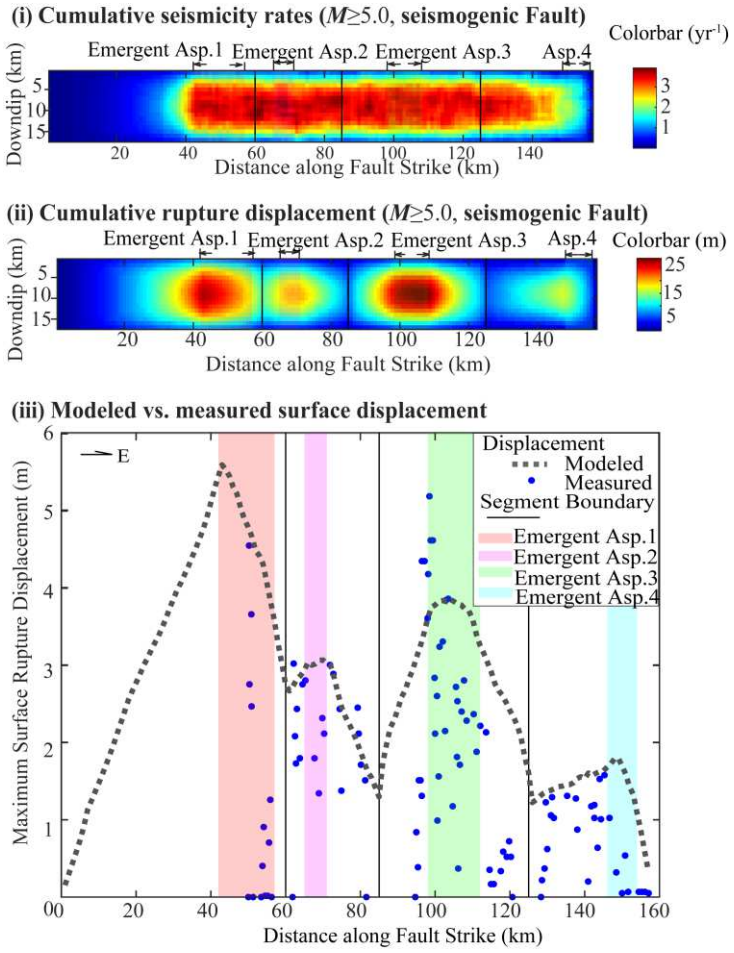
Extended Data Fig. 13 Asperity-controlled rupture and surface displacement for 1992 *M*w7.3 Landers Earthquake, USA. Panels show (i) modeled surface rupture displacement, (ii) corresponding fault-plane displacement prior to near-surface adjustment, and (iii) cumulative along-strike seismicity rate.



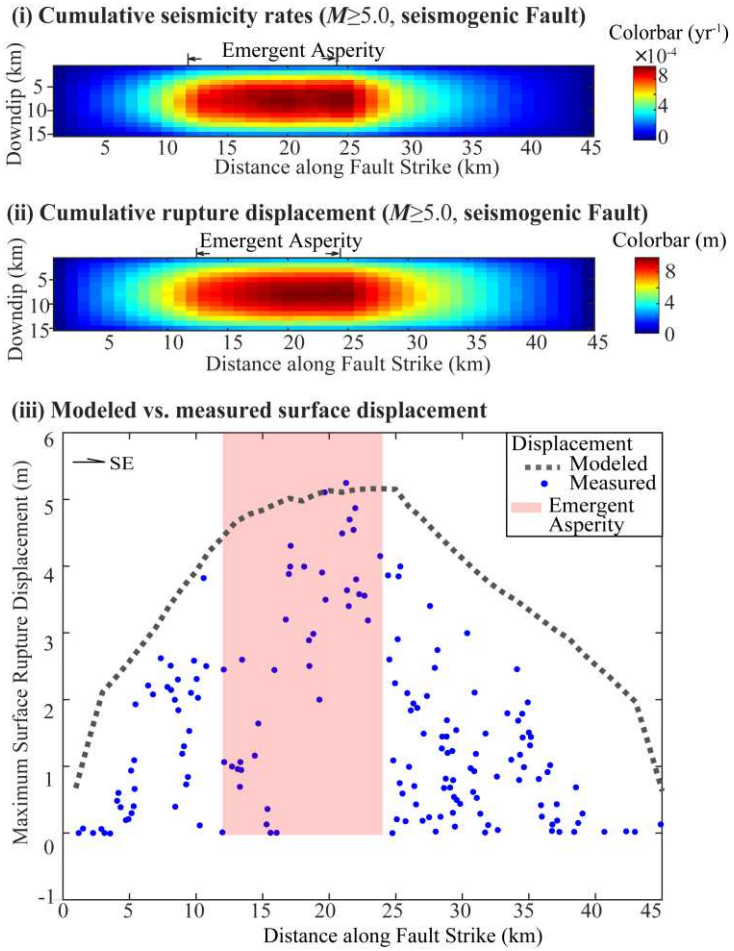
850

851 **Extended Data Fig. 14 Asperity-controlled rupture and surface displacement**
852 **for 1997 *M*w7.5 Manyi Earthquake, China.** Panels show (i) modeled surface rupture
853 displacement, (ii) corresponding fault-plane displacement prior to near-surface
854 adjustment, and (iii) cumulative along-strike seismicity rate.

855



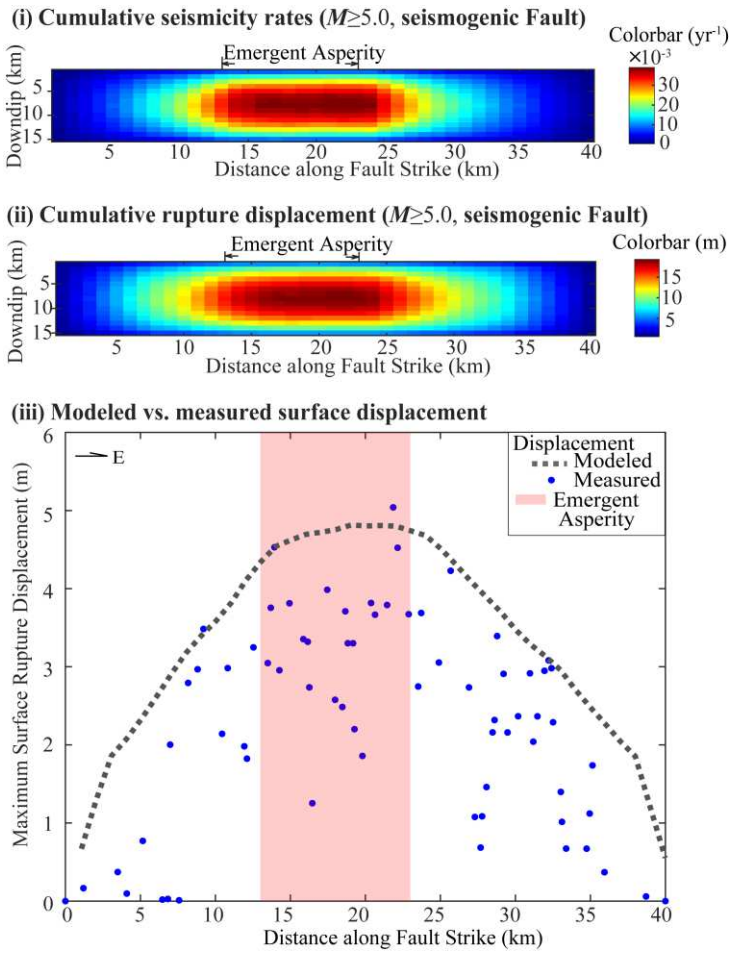
Extended Data Fig. 15 Asperity-controlled rupture and surface displacement for 1999 *M*w7.6 Izmit Earthquake, Türkiye. Panels show (i) modeled surface rupture displacement, (ii) corresponding fault-plane displacement prior to near-surface adjustment, and (iii) cumulative along-strike seismicity rate.



862

863 **Extended Data Fig. 16 Asperity-controlled rupture and surface displacement**
864 **for 1999 *M*w6.9 Hector Mine Earthquake, USA.** Panels show (i) modeled surface
865 rupture displacement, (ii) corresponding fault-plane displacement prior to near-surface
866 adjustment, and (iii) cumulative along-strike seismicity rate.

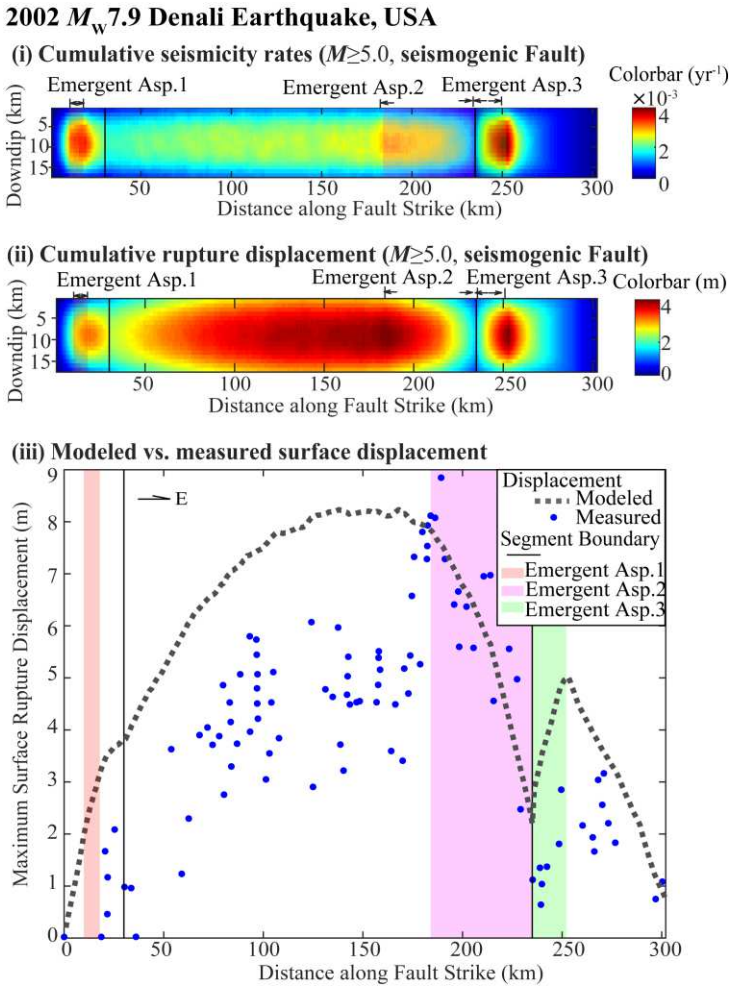
867



868

869 **Extended Data Fig. 17 Asperity-controlled rupture and surface displacement**
870 **for 1999 *M*w7.0 Duzce Earthquake, Türkiye.** Panels show (i) modeled surface
871 rupture displacement, (ii) corresponding fault-plane displacement prior to near-surface
872 adjustment, and (iii) cumulative along-strike seismicity rate.

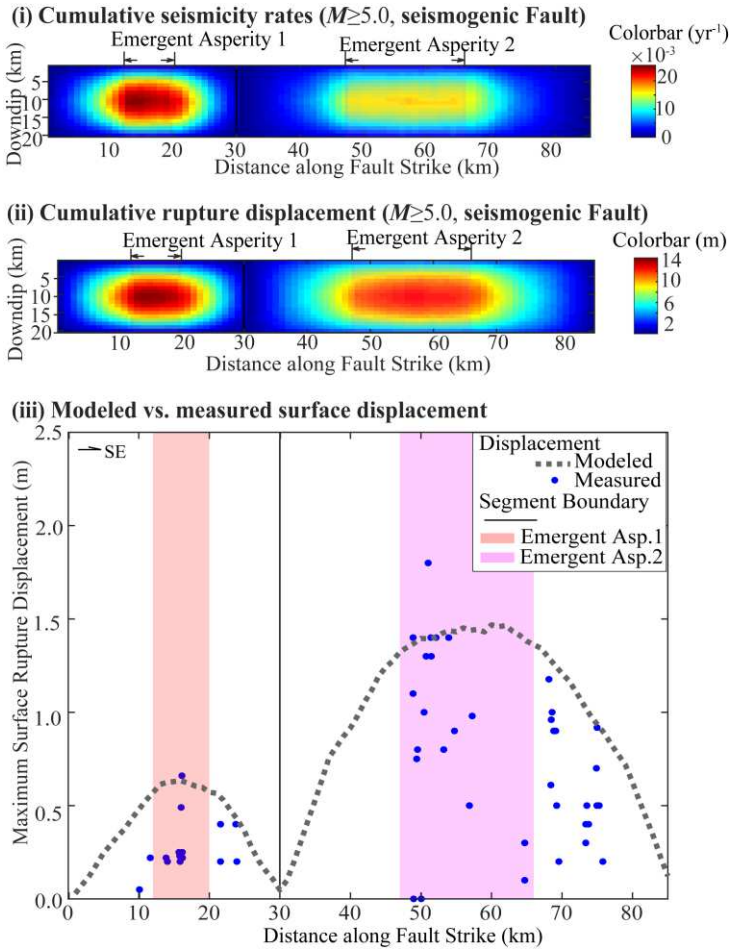
873



874

875 **Extended Data Fig. 18 Asperity-controlled rupture and surface displacement**
876 **for 2002 *M*w7.9 Denali Earthquake, USA.** Panels show (i) modeled surface rupture
877 displacement, (ii) corresponding fault-plane displacement prior to near-surface
878 adjustment, and (iii) cumulative along-strike seismicity rate.

879



880

881 **Extended Data Fig. 19 Asperity-controlled rupture and surface displacement**
882 **for 2010 *M*w6.9 Yushu Earthquake, China.** Panels show (i) modeled surface rupture
883 displacement, (ii) corresponding fault-plane displacement prior to near-surface
884 adjustment, and (iii) cumulative along-strike seismicity rate.

885